# Low-level embryonic crude oil exposure disrupts ventricular ballooning and subsequent trabeculation in Pacific herring

John P. Incardona[1*], Tiffany L. Linbo[1], Barbara L. French[1], James Cameron[2], Karen A. Peck[1], Cathy A. Laetz[1], Mary Beth Hicks[3], Greg Hutchinson[3], Sarah E. Allan[4], Daryle T. Boyd[1], Gina M. Ylitalo[1], Nathaniel L. Scholz[1]

[1]Northwest Fisheries Science Center, National Oceanic and Atmospheric Administration, Seattle, WA USA.

[2]Earth Resources Technology, under contract to Northwest Fisheries Science Center, National Oceanic and Atmospheric Administration, Seattle, WA USA.

[3]Oregon State University, Cooperative Institute for Marine Resources Studies, Hatfield Marine Science Center, Newport, OR USA.

[4]National Oceanic and Atmospheric Administration, Office of Response and Restoration, Anchorage, AK USA.

*Author for correspondence

email: john.incardona@noaa.gov

tel: 206-860-3347

**Abstract**

There is a growing awareness that transient, sublethal embryonic exposure to crude oils cause subtle but important forms of delayed toxicity in fish. While the precise mechanisms for this loss of individual fitness are not well understood, they involve the disruption of early cardiogenesis and a subsequent pathological remodeling of the heart much later in juveniles. This developmental cardiotoxicity is attributable, in turn, to the inhibitory actions of crude oil-derived mixtures of polycyclic aromatic compounds (PACs) on specific ion channels and other proteins that collectively drive the rhythmic contractions of heart muscle cells via excitation-contraction coupling. Here we exposed Pacific herring (*Clupea pallasi*) embryos to oiled gravel effluent yielding ΣPAC concentrations as low as ~ 1 μg/L (64 ng/g in tissues). Upon hatching in clean seawater, and following the depuration of tissue PACs (as evidenced by basal levels of *cyp1a* gene expression), the ventricles of larval herring hearts showed a concentration-dependent reduction in posterior growth (ballooning). This was followed weeks later in feeding larvae by abnormal trabeculation, or formation of the finger-like projections of interior spongy myocardium, and months later with hypertrophy (overgrowth) of the spongy myocardium in early juveniles. Given that heart muscle cell differentiation and migration are driven by $Ca^{2+}$-dependent intracellular signaling, the observed disruption of ventricular morphogenesis was likely a secondary (downstream) consequence of reduced calcium cycling and contractility in embryonic cardiomyocytes. We propose defective trabeculation as a promising phenotypic anchor for novel morphometric indicators of latent cardiac injury in oil-exposed herring, including an abnormal persistence of cardiac jelly in the ventricle wall and cardiomyocyte hyperproliferation. At a corresponding molecular level, quantitative expression assays in the present study also support biomarker roles for genes known to be involved in muscle

46 contractility (*atp2a2*, *myl7*, *myh7*), cardiomyocyte precursor fate (*nkx2.5*) and ventricular
47 trabeculation (*nrg2*, and *hbegfa*). Overall, our findings reinforce both proximal and indirect roles
48 for dysregulated intracellular calcium cycling in the canonical fish early life stage crude oil
49 toxicity syndrome. More work on $Ca^{2+}$-mediated cellular dynamics and transcription in
50 developing cardiomyocytes is needed. Nevertheless, the highly specific actions of ΣPAC
51 mixtures on the heart at low, parts-per-billion tissue concentrations directly contravene classical
52 assumptions of baseline (i.e., non-specific) crude oil toxicity.

## 1. Introduction

As forage fish, Pacific herring (*Clupea pallasi*) are a keystone species for food webs in the northern Pacific Ocean and the Bering Sea (McKechnie et al., 2014). They spawn adhesive, demersal embryos on nearshore vegetation and other substrates and are therefore susceptible to developmental toxicity from shoreline pollution. This is particularly true for oil spills, including the 1989 Exxon Valdez and the 2007 Cosco Busan oil spills. These surface spills from grounded ships oiled the nursery habitats for herring shortly before the annual spawning seasons in Prince William Sound and San Francisco Bay, respectively. Following the Exxon Valdez spill, field collections of herring larvae that hatched along oiled shorelines identified an injury syndrome of developmental abnormalities typified most prominently by pericardial and yolk sac fluid accumulation (edema or "ascites"; Marty et al., 1997). Subsequent laboratory studies using an exposure system designed to emulate an oiled shoreline (effluent from oiled gravel columns) linked this syndrome to the bioconcentration of polycyclic aromatic hydrocarbons (PAHs), or more specifically, polycyclic aromatic compounds (PACs), a broader term that encompasses related heterocyclic compounds (Carls et al., 1999). The 2007 Cosco Busan bunker spill involved a different type of oil – namely, the bunker fuel used to power large marine vessels worldwide. Crude and bunker oils represent the beginning and end of the refinement process, respectively, and therefore have different chemical compositions (Uhler et al., 2007; Wang et al., 2003). Specifically, fuel oil is a residual and highly viscous fraction enriched in many contaminants with as-yet uncharacterized chemical and toxicological properties. The Cosco Busan oil proved highly lethal to herring embryos and larvae by a process involving photosensitization (Hatlen et al., 2010; Incardona et al., 2012b). This was in addition to the canonical cardiotoxic effects of

PACs, which were evident as edema in caged (submerged) embryos and natural spawn up to two years after the spill (Incardona et al., 2012a).

For every fish species tested, embryonic exposure to crude oil leads to a syndrome of embryo-larval heart failure, marked by the accumulation of edema. This has been observed for an extensive diversity of freshwater and marine fish, exposure methods and geological sources of crude oil and its refinery fuel products (e.g., Adeyemo et al., 2015; Jung et al., 2017; Li et al., 2018; Linden, 1978; Madison et al., 2017; Pollino and Holdway, 2002; Raine et al., 2017). Studies over the past 15 years on Pacific herring and several other select species have identified specific aspects of cardiac failure as the central etiology of this crude oil developmental toxicity syndrome (reviewed by Incardona and Scholz, 2018; Incardona, 2017; Incardona and Scholz, 2016). Along a concentration-response gradient, exposures to petrogenic mixtures containing PACs at relatively high and yet environmentally-relevant levels (i.e., water concentrations of $\gtrsim$ 10 µg/L $\sum$PACs producing tissue levels of $\gtrsim$ 1000 ng/g wet weight) cause severe heart malformation, secondary extracardiac defects, and embryolarval lethality (e.g., Esbaugh et al., 2016; Incardona et al., 2009; Incardona et al., 2005; Incardona et al., 2004; Incardona et al., 2014; Jung et al., 2015; Morris et al., 2018; Sørhus et al., 2016b). At lower concentrations (i.e., $\lesssim$ 1 µg/L $\sum$PACs in water producing $\lesssim$ 200 ng/g wet weight in tissues), embryos survive transient cardiac dysfunction but subsequently grow poorly as juveniles with reduced survival rates (Heintz, 2007; Heintz et al., 2000; Incardona et al., 2015). Importantly, these survivors had subtle abnormalities in cardiac structure indicative of pathological remodeling, including altered ventricular shape, reduced compact myocardium, and hypertrophic spongy myocardium. These adverse anatomical changes were coupled in turn with reduced cardiorespiratory performance, as measured by lower critical swimming speeds (Hicken et al., 2011; Incardona et al., 2015).

98 Consistent with these structural and functional abnormalities, transcriptome sequencing of
99 isolated juvenile pink salmon (*Oncorhynchus gorbuscha)* hearts revealed changes in the
100 expression of genes involved in cardiomyocyte proliferation and hypertrophy (enlargement or
101 overgrowth), inflammation, and innate immunity (Gardner et al., 2019).
102 It is well established that cardiac function and form are inextricably interdependent processes
103 that together shape heart development in fish and other vertebrates (for review see Andrés-
104 Delgado and Mercader, 2016; Miquerol and Kelly, 2013). In this context, it has been shown that
105 3-ring classes of PACs that are commonly enriched in crude oil (e.g., the tricyclic
106 phenanthrenes) directly and specifically interfere with cardiac function. This is evidenced by the
107 disruption of cyclical action potential generation and intracellular calcium cycling in isolated
108 heart muscle cells, or cardiomyocytes (Brette et al., 2014; Brette et al., 2017). These twin effects
109 underlie the whole-heart phenotypes of 1) heart rate and rhythm defects and 2) reduced
110 contractility observed in developing embryos (Edmunds et al., 2015; Incardona et al., 2009;
111 Incardona et al., 2004; Incardona et al., 2014; Incardona et al., 2013; Jung et al., 2013; Morris et
112 al., 2018; Sørhus et al., 2016b). Developmental genetics in zebrafish have clearly demonstrated a
113 role for cardiac function in multiple aspects of late cardiogenesis, including chamber looping,
114 initial proliferation of ventricular cardiomyocytes, outgrowth of the ventricule (ballooning) and
115 formation of the internal spongy myocardium (trabeculation) (e.g., Berdougo et al., 2003;
116 Dietrich et al., 2014; Jimenez-Amilburu et al., 2016; Rasouli and Stainier, 2017; Rottbauer et al.,
117 2001); for a recent review, see (Sidhwani and Yelon, 2019). Intracellular $Ca^{2+}$ handling is
118 particularly central to many of these morphological processes, presumably via excitation-
119 transcription coupling (reviewed by Ljubojevic and Bers, 2015; Wamhoff et al., 2006).
120 Hypothesis-driven and exploratory transcriptome analyses of several marine fish embryos

121 exposed to crude oil have identified changes in the expression of genes critical for
122 cardiomyocyte $Ca^{2+}$ dynamics, as well as transcription factors and signaling molecules with
123 known roles in heart development (Edmunds et al., 2015; Sørhus et al., 2017; Sørhus et al.,
124 2016b; Xu et al., 2016). At the upper end of the concentration-response relationship ($\gtrsim$ 10 µg/L
125 ∑PACs), the crude oil cardiotoxicity syndrome mimics genetic loss-of-function in zebrafish
126 (e.g., Arnaout et al., 2007; Ebert et al., 2005; Rottbauer et al., 2001), leading to complete heart
127 failure and death soon after hatching (e.g., Esbaugh et al., 2016; Khursigara et al., 2017; Laurel
128 et al., 2019). For wild fish that spawn in more lightly oiled habitats, uncertainty remains with
129 respect to the mechanisms and processes that extend from mild functional impairment in
130 transiently-exposed embryos to delayed toxicity in the form of altered cardiac structure and
131 performance in surviving larvae, juveniles, or adults. Such latent impacts have been initially
132 investigated in zebrafish (Hicken et al., 2011) as well as Pacific herring and pink salmon
133 (Incardona et al., 2015).
134 Here we conducted a detailed anatomical and functional investigation of the hearts of Pacific
135 herring through the larval and early juvenile stages following embryonic exposure to trace levels
136 of crude oil. We specifically focused on circulatory-dependent morphogenetic processes that
137 give rise to the fine structure of the developing ventricle, including the expression of genes
138 known to be involved in the shape, orientation, and migration of ventricular cardiomyocytes
139 during the major windows for initiation of ventricular ballooning and trabeculation). Lastly, we
140 identify potentially novel molecular indicators at the embryonic stage that presage latent,
141 abnormal cardiac remodeling in response to sublethal oil toxicity. These findings substantively
142 refine and extend our current understanding of the PAC-driven adverse outcome pathway(s) in

developing fish, and suggest new tools for measuring contaminant exposure and injury in the aftermath of future oil spills.

## 2. Materials and methods

*Herring collection and fertilization*. Ripe herring were captured from spawning aggregations by hook and line March 3, 2016 in Yaquina Bay, Newport, OR under Oregon Department of Fish and Wildlife permit #20039. Ovaries and testes were dissected and stored on ice in humidified 100 mm plastic Petri dishes until fertilization. The average mass of ovaries (mean ± S.D.) was 19.3 ± 5.2 g from 46 females with a fork length of 18.8 ± 1.0 cm and a total body mass of 81.4 ± 13.6 g. The corresponding weight of testes averaged 16.8 ± 5.3 g from 26 males with a fork length of 19.3 ± 1.0 cm and a total body mass of 81.0 ± 11.8 g. Fertilizations were carried out as detailed elsewhere (Griffin et al., 1998), using polyvinyl alcohol to prevent the clumping of eggs as they were distributed onto each of 16 sheets of 1 mm nylon mesh. Each 21x24 cm sheet held 10–20 g of embryos from 3–4 pooled females and two pooled males. Fertilizations were completed within a 3 hr period, and eggs were held overnight in a 4 ft tank supplied with 10ºC seawater. Subsequent microscopic assessment confirmed a successful fertilization rate of 76.2 ± 8.5%.

*Exposure to oiled gravel effluents*. Exposures were carried out at the NOAA Northwest Fisheries Science Center's Newport Research Station at the Hatfield Marine Science Center (Newport, OR) using filtered seawater pumped from adjacent Yaquina Bay maintained at 10ºC. Oiled gravel was prepared using artificially weathered Alaska North Slope crude oil as previously described (Incardona et al., 2012b). Gravel was coated with oil in a dosing series of 0.25, 0.5,

166 and 1.0 g mass of oil per kg gravel. Columns were constructed using polyvinyl chloride plastic
167 pipe (9.6 cm diameter) cut into 58 cm-tall sections and filled with ~ 1100 $cm^3$ of gravel. Water
168 flow through each column (3.5 L/h) was vertical from an inflow at the base to an outflow at the
169 top collected into individual 75-L glass aquaria fitted with outflow bulkheads to maintain a
170 steady-state volume of ~ 68 L. A total of 16 columns were used, including n = 4 replicates of
171 clean gravel (control treatment) and each of the three oil mass doses. Temperature in the
172 exposure effluents was controlled by placing the aquaria in a water table supplied with high-
173 flow, 10ºC seawater. The outflow from each aquarium was collected and decontaminated with
174 activated charcoal. Embryos were exposed to column effluents beginning at 24 hr post-
175 fertilization by vertically suspending the mesh sheets. Overall experimental design for exposure,
176 transfer to clean water, post-exposure growth, all sample types and sampling points is provided
177 in Fig. S1. Samples collected for lipid analyses were used to obtain dry weight values, but
178 otherwise are the subject of a separate report.
179
180 *Larviculture*. Upon completion of the exposure window prior to hatching (10 dpf), each strip of
181 remaining mesh with adhering embryos was cut into two equal pieces and transferred to the
182 bottom of duplicate 400 L cylindrical flow-through fiberglass tank fitted with black plastic
183 lining. Herring larvae hatched between 12 and 15 dpf. Hatching was quantified at 15 dpf by
184 collecting 12 random images of each mesh and counting empty chorions and total embryos in
185 each image. Total hatch per sheet was calculated as the mean percent empty chorions (N = 12),
186 and the overall hatch per treatment calculated as the mean of the 4 sheets per dose. Clean
187 seawater was supplied (1 - 5 L per min) through a submerged spray bar positioned at an angle
188 near the bottom of the tank to minimize disturbance to the larvae. Additional water column

circulation was provided by an air stone, and tanks were maintained at 10° C. Larvae were exposed to a light regimen consistent with ambient local conditions via skylight, supplemented by fluorescent lighting for 8:16 h light:dark. Larvae were fed live rotifers and brine shrimp. Rotifers (*Brachionus plicatilis*) were cultured in filtered and aerated seawater at 25-28 °C, pH = 6.7-8.5, and a salinity 18-22 ppt adjusted using dechlorinated municipal freshwater. Brine shrimp (*Artemia*) were cultured in seawater with 0.75 g/L sodium bicarbonate at 25-30 °C, pH = 8.0-8.5, salinity = 25-35 ppt, and a 2000 lux light intensity. Rotifers were enriched to 0.3 g/million for 8-16 hrs with Algamac (BioMarine) and *Artemia* were enriched to 0.5 g/L for 24 hrs with S.presso (Selco). Triplicate counts for either prey were determined daily via compound microscope, with feed volumes adjusted as needed to meet targeted densities.

Herring larvae were fed enriched rotifers from days 2-30 post-hatching at a density of 5 prey/ml (500,000 rotifers per 100 L seawater) twice daily. From days 5-124, larvae were fed enriched *Artemia* twice daily at a density of 2-4 prey/mL. To improve the visual contrast for larval capture of rotifer and shrimp prey, green water (Roti-grow Green, Reed Mariculture) was added to each grow-out tank prior to feeding. Beginning at 73 days post-hatch, herring larvae were transitioned to a custom trout feed (< 600 µm pellet size; Rangen) at a rate of twice daily. Individual tanks were cleaned weekly by siphoning.

*Analysis of PACs in water and embryo tissues*. Water samples (200 mL) were collected by glass pipet at exposure days 1 and 10, stabilized by the addition of 20 mL dichloromethane, and stored in glass amber bottles at 4ºC. At exposure day 10, ~ 1–2 g embryos were removed from each mesh, placed in pre-cleaned 125 mL glass I-CHEM jars (300 series; VWR Scientific), and stored at –20 ºC until analysis. Forty two PAC analytes were quantified (Data S1) as detailed previously

(Sloan et al., 2014). In brief, samples were extracted with methylene chloride using separatory funnels (water) or an accelerated solvent extractor (tissue). PAC extracts were subsequently cleaned up by silica/aluminum columns (to remove highly polar compounds) and size-exclusion high-performance liquid chromatography (to remove lipids) before final quantification. The PACs were then separated on a 60 m DB-5 gas chromatography (GC) capillary column for detection on an electron impact mass spectrometer (MS) in selected-ion monitoring mode. In cases where a PAC compound was not detected in a sample, the value was reported as "less than the limit of quantification", or "<LOQ". A LOQ concentration was calculated for each sample based on sample mass and instrument performance for each batch of samples. Summed PAC concentrations (ΣPACs; see below) were calculated from detected values only. Complete PAC data are provided in supplemental file Data S1.

*Sampling and live imaging of embryos and larvae.* For gene expression analyses, embryos were sampled every other day during exposures (2, 4, 6, 8, and 10 dpf). A section was trimmed from each mesh and 20 embryos per exposure replicate (4 replicates per treatment) were removed after confirmation of viability via stereomicroscope inspection. After hatch (14 dpf), free-swimming yolk-sac larvae (20 per replicate) were randomly captured from the water column by wet bailing and concentration in cell strainers (Falcon 100 µm mesh, VWR #21008-950), anesthetized with MS-222, and transferred to sample collection tubes. Embryos and larvae were flash frozen on liquid nitrogen and stored at -80 ºC until extraction.

For phenotypic quantification after hatch, yolk sac larvae were randomly captured from each replicate tank, concentrated in cell strainers, and anesthetized with MS-222 titrated to inhibit a touch response. For each replicate, 30 larvae were mounted laterally (anterior to left) in 100-mm

petri dishes filled with agarose containing slots molded into it by glass capillary tubes. Petri dishes were filled with seawater and maintained at 12 ºC using Peltier-cooled microscope stages (Brook Industries, Lake Villa, IL). Ten second digital video clips were collected for each larva focused on the heart region using the highest magnification on Nikon SMZ-800 stereomicroscopes fitted with Unibrain Fire-i780c cameras (Unibrain.com), connected via firewire to a laptop computer with the BTV Pro application (Bensoftware.com). For each replicate, several larvae were selected at random for representative composite images of the entire animal. Using two imaging stations, 480 larvae were imaged over an 8-hour period, with all dose levels randomized throughout. After imaging, larvae were collected into sample tubes (30 per tube) fixed for several hours in 4% Millinog's phosphate-buffered paraformaldehyde, rinsed in phosphate-buffered saline (PBS), and then transferred into methanol and stored at -20 ºC. Similar methods were used to capture digital images and video from and subsequently fix representative larvae for each treatment at 20 and 67 dpf. At 125 dpf, fish were sacrificed by MS-222 overdose and the hearts dissected in herring Ringer's solution, immediately digitally photographed in the lateral and dorsal views using Nikon SMZ-800s, and then fixed in Dietrich's solution overnight and stored in 70% ethanol at – 20ºC. Fork length (FL) and weight (W) were collected for each fish at 125 dpf, and these measures used to calculate the condition factor K, using the formula $K = FL\ (cm) / W(g)^3 \times 100$.

*Antibody labeling and imaging.* For 67 dpf samples, whole herring larvae were rehydrated from storage in fixative via a graded methanol-PBS series. The trunk was then transected just posterior to the heart to facilitate whole mount immunolabeling. Head structures were subsequently permeabilized with distilled water (10 min) followed by several hours incubation in PBS + 0.1%

Triton X-100 (PBT) with 3% normal goat serum. The tissues were then incubated overnight at room temperature in an anti-myosin heavy chain monoclonal antibody MF20 (Developmental Studies Hybridoma Bank, University of Iowa) at 1 µg/mL. After three PBT washes (several hours each), the samples were incubated overnight in AlexaFluor-568-conjugated goat-anti-mouse $IgG_{2b}$ secondary antibody (ThermoFisher Scientific), cleared in 50% glycerol/PBS, and then labeled with 300 nM DAPI (20 min). Finally, whole hearts were carefully dissected from the head structures and mounted under a coverslip either laterally or ventral side up in 3% methylcellulose. Fluorescence was imaged using a Zeiss LSM5 Pascal confocal system with 405 and 543 nm laser excitation lines.

Hearts dissected from 125 dpf fish were embedded in paraffin and sectioned at 5 µm thickness. Slides were de-paraffinized in xylene substitute, hydrated through an alcohol series, and rinsed with $dH_2O$. Antigen unmasking was performed by heating tissue sections at 94 – 99°C in buffer containing 10 mM sodium citrate and 0.05% Tween 20, pH 6.0, for ten minutes, followed by cooling at room temperature for thirty minutes. In a room temperature humidity chamber, slides were treated for 5 min with PBS, then 30 min with block solution (PBS, 0.1% Triton X-100, 5% heat-inactivated normal goat serum, 1% DMSO, and 0.02% sodium azide), then overnight with primary antibody (anti-myosin heavy chain, MF20) at 1 µg/ml in block solution. This was followed by three washes for five minutes each with PBST (PBS and 0.1% Tween X-100), then overnight incubation with secondary antibody (goat anti-mouse IgG Alexa Fluor 488, ThermoFisher Scientific #A-11001) diluted 1:2,000 in block solution. Slides were then washed three times for five minutes each with PBST, and five minutes with PBS. Nuclei were stained with 600 nM DAPI (Invitrogen #D3571) in PBS for five minutes, followed by three rinses with PBS. Slides were mounted in 50% glycerol in PBS and 2-3 sections per heart (6

control, 7 exposed) imaged using an AxioCam HRm digital camera and a Zeiss LSM 5 Pascal confocal system with an Ar laser. Fiji software was used to quantify the number of DAPI+ nuclei and the percent trabeculation within the ventricle. Region Of Interest selection was used to measure total ventricle area and Color Threshold analysis was used to quantify percent MF20+ ROI within the entire ventricle (percent trabeculation). Sections for imaging were selected based on similar profiles of central structures (e.g., bulbus arteriosus and atrioventricular valve).

*RNA extraction and quantitative real-time PCR*. Total RNA was extracted by homogenizing samples in TRIzol (5% v/v, ThermoFisher Scientific) and then purified with a Direct-zol™ RNA MiniPrep column (Zymo Research Cat# R2051). RNA concentrations and purities were measured using a Nanodrop ND-1000 Spectrophotometer. Superscript IV (Thermofisher Cat #18090050) with oligo dt(20) primers was used to synthesize cDNA. For characterization of cardiac target genes, hearts and swimming muscle samples were collected from each of three 1-yr old cultured juvenile fish obtained from the US Geological Survey's Western Fisheries Research Center Marrowstone Field Station.

Reverse transcriptase quantitative polymerase chain reaction (qPCR) was performed on a Viia™ 7 Real-Time PCR system with Fast SYBR Green (ThermoFisher Scientific). Gene-specific RT-qPCR primers were designed using Primer3 (http://bioinfo.ut.ee/primer3/) and synthesized by Integrated DNA Technologies, Inc. (Coralaville, Iowa). Herring-specific target sequences for primer design were identified by BLAST searches based on sequences from either an Atlantic haddock (*Melanogrammus aeglefinus*) embryonic transcriptome (Sørhus et al., 2016a; Sørhus et al., 2017) or the coding region of zebrafish genes (National Center for Biotechnology Information online database), using either an Atlantic herring (*C. harengus*)

304 genome assembly (NCBI accession number ASM96633v1; (Martinez Barrio et al., 2016) or two
305 published Pacific herring transcript libraries (Roberts et al., 2012). The herring genes identified
306 by this approach were annotated using BLAST-based sequence alignments. Primer sequences are
307 provided in Table S1.
308 Candidate reference genes were selected based on a lack of oil exposure treatment effect
309 from the previously published Atlantic haddock embryonic and larval transcriptomes (Sørhus et
310 al., 2017). These included *ef1a* (elongation factor 1 alpha), *mtm1* (myotubularin 1), *rxrba*
311 (retinoid receptor X beta a), *spop1* (speckle type BTB/POZ protein 1), and *wdtc1* (WD and
312 tetratricopeptide repeats 1). Absence of an oil exposure effect for herring orthologs of these
313 genes was confirmed by analyzing qPCR data for the current herring oil exposure using a
314 consensus of BestKeeper, GeNorm, and NormFinder algorithms with the RefFinder program
315 (Xie et al., 2012). Based on this analysis, *mtm1* was eliminated and the other four genes retained
316 (*ef1a*, *rxrba*, *spop1* and *wdtc1*). The reference gene selection approach was validated by running
317 target gene qPCR raw data through the same algorithms, which failed in each case. Due to the
318 low RNA yield of samples, primer efficiency was measured using standard curves generated
319 from cDNA synthesized from the same cohort. Primer efficiencies and $r^2$ values were within
320 acceptable range for each reference gene (Nolan et al., 2006). Normalized quantification
321 threshold (Ct) values (dCt) and fold-change values relative to controls were calculated with the
322 Comparative Ct method, using the geometric mean of the four reference genes (Schmittgen and
323 Livak, 2008).
324
325 *Data analysis and statistics.* Cardiac morphology and function were quantified from digital
326 videos collected from yolk sac larvae at hatch (14 dpf). All video files were blinded and analyzed

with ImageJ (https://imagej.nih.gov/ij/), with a consistent individual observer measuring all of the quantitative aspects of a given phenotype across replicates and treatments. Each video was carefully screened for quality criteria (e.g., alignment of specimen), and those not passing all criteria for a particular phenotype were excluded for that measure. Each endpoint was measured from a minimum of 23 larvae per replicate. Heart rates were measured by manually counting the number of complete contractions in each 10 sec video clip. The presence of edema was scored by deformation of the anterior yolk margin and increased pericardial area measured as detailed elsewhere (Incardona and Scholz, 2016). Heart chamber areas were measured with the freehand trace tool in ImageJ, at peak diastole and systole as identified by manually advancing through frames. Total areas for both chambers were measured at both phases of the cardiac cycle, while the posterior balloon portion of the ventricle was measured only at diastole. Cardiac jelly thickness was measured with the ImageJ straight line tool in the first 10 videos collected for each replicate, at the same location in the posterior ventricle and ventral wall of the atrium. Fractional shortening and AV angle were calculated from the chamber diameters as described elsewhere (Edmunds et al., 2015).

Data were analyzed by regression models using Prism 7 (GraphPad Software). Nonlinear models were used for cardiac endpoints, with specific(Edmunds et al., 2015) model parameters selected by statistical comparison. Lowest effective doses were determined by one-way ANOVA using JMP 13 (SAS Institute), with replicates nested within treatment to resolve tank effects. If a tank effect was present ($p \leq 0.05$), a one-way ANOVA was performed on replicate means. Means were compared using Dunnett's post-hoc test. Trabecular spacing data were analyzed by ANOVA with individual fish nested within treatment, followed by Dunnett's post-hoc test.

## 3. Results

*3.1. Measured PAC concentrations in exposure water and herring tissue.* As anticipated from previous oiled gravel column studies (e.g., Incardona et al., 2012b)), PAC levels were in the target range for the nominal levels of gravel coating and declined over time (Table 2 and Data S1). The initial total (∑)PAC concentrations for the 0.25, 0.5 and 1.0 g/kg oiled gravel treatments (averaged across the four replicate columns) were 1.3 ± 0.1, 1.9 ± 0.2 and 4.2 ± 0.6 µg/L, with clean gravel controls at 0.070 ± 0.002 µg/L. The PAC compositions (Fig. S2) showed a fairly weathered pattern, dominated by naphthalene and phenanthrene homologs with higher degrees of alkylation (i.e., C3- and C4-naphthalenes and C2- and C3-phenanthrenes). By the end of exposure (day 10), embryos accumulated 64 ± 10, 140 ± 36, and 238 ± 27 ng/g ∑PACs for the 0.25, 0.5 and 1.0 g/kg oiled gravel columns, respectively, with control tissue concentrations at background levels of 10 ± 1 ng/g. When corrected for embryo lipid content (Table 2), this dosing range (∑PAC ~ 4000 – 13,000 ng/g lipid) overlaps closely with previous pink salmon exposures (~ 2000 – 23,000 ng/g lipid) yielding oil-induced abnormalities in juvenile heart function, histological structure, and gene expression (Gardner et al., 2019; Incardona et al., 2015). For the low and medium column loading treatments (0.25 and 0.5 g/kg oil/gravel), the PAC patterns were shifted slightly toward a higher ratio of phenanthrenes to naphthalenes in both water and tissue (Fig. S2B and C). Overall, tissues showed proportionally higher levels of phenanthrenes compared to naphthalenes, in relation to the respective levels in water (e.g., Fig. S2D top/bottom).

*3.2. Induction of cyp1a mRNA.* To further characterize PAC uptake we examined the expression of mRNA encoding cytochrome P4501A (CYP1A), the primary PAC-metabolizing enzyme that

373 is induced following PAC binding to the intracellular aryl hydrocarbon receptor. Levels of *cyp1a*
374 mRNA induction were quantified in embryos throughout exposure at 6, 8 and 10 dpf, and at 14
375 dpf after four days of subsequent development and hatching in clean water. While the time
376 course of *cyp1a* expression is detailed further below in the context of cardiac gene expression
377 (Fig. 7A), maximal expression was observed at 10 dpf, with 10 ± 2 , 33 ± 5 and 55 ± 8 fold-
378 change induction relative to controls, respectively, corresponding to the 64, 140, and 238 ng/g
379 doses. Notably, by 2 dph (4 days post-exposure), *cyp1a* levels declined to control levels across
380 all doses (Fig. 7A).
381
382 *3.3. Gross body morphology and incidence of edema*. Oil exposure had no effect on hatch rates.
383 After a hatching period of three days (15 dpf), mean hatch rates for control, 64, 140, and 238
384 ng/g doses were 83.5 ± 2.8, 88.1 ± 3.1, 90.0 ± 4.0, and 82.0 ± 7.6%, respectively (ANOVA p =
385 0.5). As observed previously across many species, trace oil exposures at the lower end of the
386 concentration-response relationship yielded hatched larvae that appeared overtly normal, aside
387 from mild-moderate pericardial edema (Fig. 1). A few larvae from the 238 ng/g dose showed
388 mild dorsal curvature (Fig. 1D), but this was not frequent enough to quantify. As expected,
389 newly hatched larvae displayed dose-dependent pericardial edema, with an $EC_{50}$ of 244 ng/g
390 ∑PAC (Fig. 1E). Despite the apparent shorter length of randomly selected oil-exposed larvae
391 (e.g., Fig. 1B, C), there was no significant effect of exposure on the mass of embryos at exposure
392 day 10 or newly hatched yolk-sac larvae (14 dpf), as determined by dry weight (Fig. 1F). At the
393 first-feeding stage, after the absorption of yolk, there was a trend (p = 0.09) of reduced size in
394 larvae from oil exposed groups (Fig. 1F, white bars), although high mortality in the 238 ng/g
395 dose groups precluded sampling for dry weights.

*3.4. Cardiac function and shape in yolk sac and first-feeding larvae.* Similar to other marine species, the herring heart at late embryonic stages (e.g., 10 dpf) has a predominantly lateral orientation, with the opening of the atrium (sinus venosus) on the left side of the embryo and the ventricle to the right and slight anterior of the atrium (Fig. 2A). By the early yolk sac larval stage, the heart has migrated such that both chambers are aligned along the midline, with the atrium superior to the ventricle. The ventricle then begins to extend beneath the atrium posteriorly as an outgrowth or "ballooning" of the outer curvature (Fig. 2B). Oil exposure led to a dose-dependent decrease in ventricular ballooning measured at 14 dpf, or hatching day 2, four days post-exposure in clean seawater (Fig. 2C – E; Fig. 4A). Ventricular ballooning was highly sensitive to oil exposure, with significant reduction occurring at the 64 ng/g dose treatment and an $IC_{50}$ of ∑PAC 87 ng/g (Fig. 4A). Ventricular ballooning continued in feeding stage larvae (20 dpf or 8 days post-hatch; dph), with posterior growth in controls extending past the cleithrum (Fig. S3A, C). In larva exposed to the 238 ng/g dose, ventricular ballooning had initiated by this stage, but in contrast to controls, had not yet extended to reach the cleithrum (Fig. S3B, D).

Delayed ventricular ballooning also correlated with an increase in the thickness of cardiac jelly, the clear extracellular matrix that lies between the endocardium and myocardium in the embryonic heart. At 14 dpf/1 dph, this was particularly evident in the posterior ventricle (Fig. 3). In control yolk sac larvae, the atrial wall is much thicker than the ventricular wall (e.g., 21.4 ± 0.6 µm vs. 8.8 ±0.6 µm, respectively), largely due to more abundant cardiac jelly in the former (Fig. 3A, A'). Oil exposure led to a dose-dependent increase in the thickness of both chamber walls, visible in larvae from the 238 ng/g dose as a marked increase in ventricular cardiac jelly (Fig. 3B, B'). The increase in cardiac jelly was significant at the 64 ng/g dose ($p = 0.03$) for the

ventricle and at the 140 ng/g dose ($p = 0.006$) for the atrium, with ventricular and atrial $EC_{50}$s at 103 ng/g and 222 ng/g tissue ∑PACs, respectively (Fig. 3C). In addition, oil exposure was also associated with the appearance of a "cap" or cellular thickening of the posterior ventricular wall (Fig. S4A, B), which was dose-dependent and occurred in up to 14.2 ± 4.3% of newly hatched larvae from the 238 ng/g dose (Fig. S4C). Whole-mount labeling of hearts with anti-myosin heavy chain antibodies followed by confocal microscopy demonstrated that these cellular caps represented solid, disorganized clusters of cardiomyocytes (Fig. S4D – F).

Other morphological changes included an impact on looping of the cardiac chambers. The atrioventricular (AV) angle was decreased in oil-exposed larvae (Fig. 4B), indicating abnormal looping. This was significant at the 140 ng/g dose, with an $IC_{50}$ across treatments of 41 ng/g. In addition, an increase in the area of the atrium (Fig. 4C; blue shades) paralleled the decreased ventricular area (Fig. 4C; orange shades). The effect on atrial size was as sensitive as the reduced ventricular ballooning – i.e., significant in response to the lowest treatment. Importantly, the relationship between oil exposure and heart chamber area appeared the same for both diastolic (relaxed) and systolic (contracted) states. When the total area of the ventricle was measured, the effect was not as profound as on only the posterior ballooning portion (Fig. 4C; orange shades; compare to Fig. 4A), with only the highest dose significantly different than control. Finally, measurement of fractional shortening (Fig. 4D) showed a dose-dependent decrease in atrial contractility, but no effect on ventricular contractility. In contrast, there was no significant dose-dependent effect on heart rate at this stage, with rates for control, 64, 140, and 238 ng/g doses at 103 ± 5, 102 ± 6, 106 ± 4 and 100 ± 6 beats/min, respectively (ANOVA $p = 0.9$).

*3.5. Defective ventricular trabeculation in late larvae*. At 67 dpf there were ~200 surviving larvae in the control group, ~300 each for the 64 ng/g and 140 ng/g doses, and 62 for the 238 ng/g dose. Fish were approaching metamorphosis and appeared grossly indistinguishable by treatment (Fig. 5A, B). Cardiac structure was examined in subsamples of the 64 ng/g and 140 ng/g dose groups, but not in the 238 ng/g dose group due to low numbers. To assess internal anatomy, hearts were whole-mount labeled with anti-myosin heavy chain antibody and imaged by confocal microscopy. At this stage, the ventricles still consisted of an outer, single layer of cortical cardiomyocytes with distinct, regularly spaced trabeculae (early bands of spongy myocardium) circumferentially arranged around the anterior-posterior axis and extending between the dorsal and ventral walls. Spacing between trabecular bases that extended from the cortical layer averaged 4.7 ± 0.2 µm in controls (Fig. 5C, top). While the trabecular spacing was unchanged for herring larvae in the 64 ng/g dose group (Fig. 5C, middle, also 4.7 ± 0.2 µm), there was a significant increase in the spacing between trabeculae at the 140 ng/g dose, at 5.6 ± 0.3 µm ($p = 0.003$; Fig. 5C, bottom). Unaltered trabecular spacing in the lowest dose group notwithstanding, all oil-exposed fish (5/5 fish examined for each dose) showed a distinctive change in the distribution of myosin heavy chain labeling, with the 64 ng/g and 140 ng/g treatments both showing highly irregular spherical or ovoid aggregations, as opposed to the more linear, fibrillar arrangements in controls (Fig. 5C). Labeling of nuclei with DAPI suggested that these spheroid/ovoid aggregates may represent individual cardiomyocytes with a rounder rather than elongated form (Fig. 5D, E). These abnormal forms were found not just near the cortical layer, but were present throughout the entire extent of the trabeculae (Fig. 5D, E).

*3.6. Trabecular hypertrophy in early juveniles*. At 125 dpf, the only surviving herring belonged to the control and 64 ng/g dose groups. Although there were no significant differences in length or mass (wet weight) between these two groups, the condition factor (K, a measure of length-weight proportionality) of the oil-exposed juveniles was 18% higher (0.32 vs. 0.39; Table 3). Dimensions of the ventricle were measured in ventral and lateral images collected after fixation, across the control and low oil groups, and gross heart anatomy was superficially very similar (Fig. 6A, B). Moreover, there were no significant differences in either the lateral or ventral areas of the ventricle (Table 2). However, while there was no significant difference in the ventral aspect ratio, the lateral aspect ratio was reduced from 2.17 ± 0.05 in controls to 1.91 ± 0.04 in the low dose group ($p = 0.0002$; Table 2). A relationship between ventricular shape, K, and swimming performance has been described for juvenile salmonids (Claireaux et al., 2005), with fish with higher K having rounder hearts and slower critical swimming speed. Similarly, in control herring at 125 dpf, there was a strong relationship between increasing K and decreased aspect ratio (rounder hearts) (Fig. 6C, circles; $r^2 = 0.6$, $p = 0.01$). However, in fish from the 64 ng/g dose group, there was no relationship between K and ventricular aspect ratio (Fig. 6C, squares.)

Trabecular structure was assessed in histological sections of the same hearts. Sections of control hearts at 125 dpf labeled with anti-myosin heavy chain generally showed an internal spongy myocardium consisting of a finely ordered meshwork of trabeculae, interspaced with prominent lumina of roughly equal area (Fig. 6D). In contrast, hearts from the 64 ng/g dose group showed denser, more irregular trabeculae with less pronounced luminal spaces between them (Fig. 6E). To determine if this represented a hypertrophic response to crude oil, we quantified the area occupied by trabecular cardiomyocytes by measuring pixels from anti-myosin

heavy chain immunofluorescence, and assessed cellularity by counting nuclei stained with DAPI (Fig. 6F). Importantly, aggregate nuclei enumeration is a potentially indeterminate indicator of myocyte-specific toxicity as it is not possible to distinguish among nuclei in cardiomyocytes, endothelial cells, fibroblasts, erythrocytes or other cell types present in the ventricle. Nevertheless, normalizing the total count of nuclei to the area occupied by anti-myosin heavy chain labeling showed a trend of lower density for the exposed fish. While this was not statistically significant, this is suggestive of larger cardiomyocyte size in the oil exposed group. On the other hand, the total area occupied by trabecular myosin heavy chain labeling in the 64 ng/g dose group was increased significantly by 7% (55.4 ± 1.9% vs. 48.5 ± 2.0%; $p = 0.04$). This indicates, conversely, that the luminal space available for ventricular filling was reduced from approximately 51.5% to 44.6% in oil-exposed fish.

*3.7. Changes in the expression of genes involved in cardiac $Ca^{2+}$ handling, contractility, ventricular specification and trabeculation.* We examined the transcription of four types of genes premised on the known effects of oil exposure on cardiac gene expression in mahi mahi (*Coryphaena hippurus*) (Edmunds et al., 2015; Xu et al., 2016) and Atlantic haddock (Sørhus et al., 2017; Sørhus et al., 2016b)), as well as previous studies of normal trabeculation in zebrafish (Rasouli and Stainier, 2017; Samsa et al., 2016). This included intracellular $Ca^{2+}$ handling (*atp2a2*, encoding SERCA2; *nac2*, encoding NCX2; and *ryr2*, encoding the ryanodine receptor 2 isoform), cardiac contractility (*myl7*/*cmlc2*, encoding the cardiac myosin light chain regulatory subunit, and *myh7*, encoding ventricular myosin heavy chain), the primary ventricular cardiomyocyte determination factor *nkx2.5*, and genes identified in zebrafish that function in trabeculation (*notch1*, *nrg2*, encoding neuregulin2, and *hbegfa*, encoding heparin-binding EGF-

like growth factor). The absence of a sequenced Pacific herring genome hindered the verification of gene identity. To characterize these genes further, we compared expression levels in cardiac ventricle relative to skeletal muscle isolated from cultured 1-yr old juvenile fish. Most target gene mRNAs showed a relative enrichment in ventricle (Table 3; based mean of 3 individuals). The putative *myh7* gene was expressed at roughly equal levels in juvenile ventricle and skeletal muscle. While the mammalian *myh7* ortholog is expressed in both cardiac ventricle and slow-twitch skeletal muscle fibers (Quiat et al., 2011), myosin heavy chain gene phylogeny and expression patterns in teleosts are extremely complicated relative to mammals (McGuigan et al., 2004). The expression of this herring myh7 ortholog at relatively high levels in juvenile swimming muscle thus does not preclude it as the primary ventricular myosin heavy chain gene. As HB-EGF has a broad tissue distribution (Raab and Klagsbrun, 1997), the *hbegfa* gene would not necessarily be expected to show cardiac-specific expression.

Gene expression was first measured in 6 dpf embryos, at the onset of eye pigmentation and a point at which the heart had a regular beat, and sequentially thereafter at 8 dpf, 10 dpf, and after hatch (14 dpf; Fig. 7). The time course of PAC exposure relative to cardiotoxic response was evident from the dynamic expression pattern for *cyp1a* (Fig. 7A). Induction of *cyp1a* mRNA in response to oil was dose-dependent at 6 dpf, with expression peaking at 10 dpf (when internal tissue PACs were measured), and falling to baseline after transfer to clean water and hatch. Importantly, *cyp1a* induction was already at levels of 10- to nearly 30-fold within six days of oiled gravel column effluent exposure, indicating considerable PAC uptake. Of the three genes encoding $Ca^{2+}$-handling proteins, only *atp2a2* was significantly affected, transiently down-regulated ~2-fold at 6 dpf (Fig. 7B), with no significant effect on either *nac2* (Fig. 7C) or *ryr2* (Fig. 7D). Genes regulating contractility were significantly affected, with *myl7* showing a

consistent trend of down-regulation, with a significant ~3-fold reduction at 8 dpf and at hatch (Fig. 7E). Similarly, *myh7* showed an overall trend of down-regulation with a significant dose-dependent effect at 8 dpf, with almost 5-fold reduction at the 238 ng/g dose (Fig. 7F). Notably, *nkx2.5* was significantly downregulated in both the 140 ng/g and 238 ng/g doses at hatch (Fig. 7G), coinciding with the small ventricle phenotype. For genes potentially involved in trabeculation, there was no significant effect on *notch1* mRNA abundance (Fig. 7H). However, there was a significant ~2-fold up-regulation of *nrg2* at 10 dpf and hatch in the 238 ng/g dose group (Fig. 7I), and a significant dose-dependent down-regulation of *hbegfa* at 6 and 8 dpf (Fig. 7J), with ~3-fold reduction in the 238 ng/g dose group. Detailed expression data are provided in Table S1.

## 4. Discussion

The edematous syndrome that follows crude oil exposure in fish embryos results from heart failure. Studies that examined cardiac function closely in exposed embryos or larvae show a variety of defects relating to either contractility or rate/rhythm or both (Incardona, 2017; Incardona and Scholz, 2016). These whole-heart functional defects were recently linked to direct effects of PAC-rich mixtures or individual PACs on single-cell cardiomyocyte action potential generation, excitation-contraction coupling, and contractility (Brette et al., 2014; Brette et al., 2017; Vehniäinen et al., 2019). In our previous studies with Pacific herring embryos, we showed that exposure to the same Alaskan crude oil used here resulted in a pronounced slowing of the heart rate (bradycardia) and reduced contractility well before hatch at 7 dpf with tissue ∑PAC concentrations of 620 ng/g (Incardona et al., 2009), about 2.5-times higher than the high dose achieved here. The data presented here now clearly link those earlier functional defects to

555 adverse effects on later morphogenetic maturation of the cardiac ventricle, at even lower doses,
556 and in the absence of other visible extra-cardiac morphological phenotypes. In newly hatched
557 larvae (14 dpf), ventricular ballooning was delayed in a manner highly dose-dependent on tissue
558 PACs, as was the concomitant reduction in ventricular wall cardiac jelly. Despite a recovery in
559 ballooning (by 20 dpf), subsequent trabeculation was dose-dependently disrupted in late larvae,
560 along with a possible abnormal increase in cardiomyocyte proliferation (67 dpf). At the lowest
561 dose tested, ∑PAC 64 ng/g wet weight, this led to hypertrophic changes within spongy
562 myocardium in early juveniles (125 dpf). These findings directly link early impairment of
563 embryonic cardiac function (contractility and fluid flow) from crude oil exposure to subsequent
564 disruption of the co-dependent, downstream processes of ventricular ballooning and
565 trabeculation in larvae and early juveniles. In turn, these defects in late steps of cardiac
566 morphogenesis set the stage for much later pathological remodeling (hypertrophy) and reduced
567 cardiorespiratory performance, as previously documented for older juvenile herring and pink
568 salmon (Gardner et al., 2019; Incardona et al., 2015) or adult zebrafish (Hicken et al., 2011).
569 In virtually every species examined, a hallmark of acute oil cardiotoxicity to embryos is
570 reduced contractility of one or both cardiac chambers (e.g., (Edmunds et al., 2015; Incardona et
571 al., 2013; Morris et al., 2018; Sørhus et al., 2016b). This reduction in contractility is consistent
572 with the rapid, direct effects of either select individual tricyclic compounds (e.g., phenanthrene)
573 or a dissolved chemical mixture from whole oil on intracellular $Ca^{2+}$ cycling in cardiomyocytes
574 (Brette et al., 2014; Brette et al., 2017). In the present study *cyp1a* levels returned to baseline
575 between the end of exposure (10 dpf) and hatching (14 dpf). This indicates that PACs were
576 depurated by the time the ventricular morphological phenotype was initially observed. Thus, a

577 transient oil-induced disruption of intracellular $Ca^{2+}$ handling subsequently disrupted ballooning
578 and trabecular morphogenesis.
579 Importantly, the observed dose-response relationships for morphological effects on the heart
580 were very robust down to low ∑PAC concentrations, specifically ~ 1 µg/L in water and 64 ng/g
581 in tissues. Based on an average molecular weight of ~200 g/mol for most petrogenic PACs, the
582 latter represents a tissue concentration of ~320 nmol/kg. This is 1,000 to 10,000-fold lower than
583 the tissue residue concentrations that have been ascribed to so-called "narcotic" or "baseline"
584 toxicity in response to acute or chronic exposures (e.g., 2 – 8 mmol/kg and 0.2 – 0.8 mmol/kg,
585 respectively; McCarty and Mackay, 1993). Instead, these tissue concentrations are consistent
586 with specific receptor interactions, as supported by the cellular studies (Brette et al., 2014; Brette
587 et al., 2017). For comparison, the $Na^+/K^+$-ATPase inhibitor digoxin affects cardiac contractility
588 (positively) at concentrations of 200 nmol/kg in myocardial tissue (Steiness and Valentin, 1976).
589 Therefore, in contrast to an adverse outcome framework premised on non-specific (or
590 unspecified) toxicological processes, the consideration of tissue PACs in the context of cardiac
591 function and heart morphogenesis is considerably more robust in terms of environmentally
592 realistic exposures, defined mechanisms of action, the extrapolation of injury across biological
593 scales, and the role of conserved evolutionary processes (e.g., calcium cycling in vertebrate
594 cardiomyocytes) as determinants of individual-based toxic response. Despite remaining
595 complexities surrounding the potency of dissolved petrogenic mixtures relative to single PAC
596 compounds, our findings support the use of tissue PAC chemistry as an environmental indicator
597 of likely toxicity to fish embryos and later life stages.
598 In the context of elucidating specific mechanisms underlying the injury phenotypes observed
599 here, relevant aspects of cardiac morphogenesis have been detailed at the organ, cellular, and

600 molecular levels in zebrafish. In particular, recent advances include a series of studies
601 elucidating the mechanisms of ventricular ballooning and trabeculation (Sidhwani and Yelon,
602 2019). All fish hearts begin as a simple linear tube, which subsequently loops (folds and twists)
603 at the AV junction to bring the atrial and ventricular chambers into an adjacent arrangement. At
604 this point, the dimensions of the two chambers are similar, and the chamber walls consist of a
605 single layer of cardiomyocytes. Subsequently, the ventricle initiates a rapid posterior expansion,
606 ballooning, that involves both rearrangement and reorientation of existing cardiomyocytes and
607 addition of new cardiomyocytes within the wall through proliferation. As ballooning progresses,
608 trabeculation begins, as cardiomyocytes from the wall project inward, delaminate and proliferate,
609 thus forming the underlying architecture of the spongy myocardium (Gupta and Poss, 2012).
610 In zebrafish, which develop more rapidly than herring (2 days to hatch vs. 12), ballooning
611 commences from the outer curvature of the ventricle nearly concomitantly with looping. These
612 initial steps of ventricular shaping and ballooning are driven by corresponding changes in the
613 shape of individual ventricular cardiomyocytes (Auman et al., 2007), and changes in the
614 orientation of neighboring cardiomyocytes within the outer curvature wall (Merks et al., 2018).
615 Changes in cardiomyocyte shape are dependent on fluid flow, and both cell shape and fluid flow
616 are dependent on actomyosin function, and by inference, intracellular $Ca^{2+}$. When either the
617 coordinated contractions of the entire ventricle or blood flow therein are reduced by disruption of
618 sarcomeric actomyosin function, ventricular cardiomyocytes fail to elongate properly (Auman et
619 al., 2007). At the same time, the function of non-muscle cytoskeletal actomyosin controls
620 cardiomyocyte shape changes through the planar cell polarity (PCP) signaling pathway, driving
621 rearrangements of neighboring cardiomyocytes during ballooning (Merks et al., 2018).

PCP signaling is mediated by non-canonical Wnt ligands acting to control the orientation of cells with respect to one another and within larger fields of cells (Yingzi and Marek, 2015). This control of cellular orientation and cell-cell associations occurs by a process involving both cell adhesion and non-muscle myosin activity, as regulated by intracellular $Ca^{2+}$ via calcium-dependent adhesion molecules (cadherins; Hale and Strutt, 2015) and the $Ca^{2+}$-dependent activation of non-muscle myosin (Somlyo and Somlyo, 2003). In zebrafish, PCP-mediated ventricular ballooning involves Wnt11 (Merks et al., 2018), a signaling protein that also regulates the conductance of $Ca^{2+}$ through L-type calcium channels during the parallel developmental coordination of electrical coupling among ventricular cardiomyocytes (Panakova et al., 2010).

The ballooning process is thus directly dependent on intracellular $Ca^{2+}$ in at least two distinct ways, whole chamber contractility driven by sarcomeric actomyosin and PCP-mediated cellular rearrangements driven by non-muscle actomyosin. The disruptive action of crude oil exposure on intracellular $Ca^{2+}$ fluxes from both internal stores (the sarcoplasmic reticulum, SR) and the extracellular electrochemical gradient (via L-type calcium channels) would thus be expected to impinge directly on the aforementioned morphogenetic processes that drive ventricular ballooning. Moreover, these morphogenetic events would be further impaired, albeit indirectly, through reductions in both fluid forces and whole chamber contractility in response to crude oil exposure. The observed recovery of ballooning over time is consistent with the depuration of PACs and consequent restoration of intracellular $Ca^{2+}$ cycling and ventricular contractility. However, our current findings show that this delay in the normal timing of ventricular outgrowth has a cascading effect on subsequent trabeculation.

644 In zebrafish, looping and the initiation of ballooning occur between ~ 36 through 48 hours
645 post-fertilization (hpf) (Glickman and Yelon, 2002; Staudt and Stainier, 2012), the
646 developmental stage also roughly equivalent to hatching in Pacific herring. Trabeculation begins
647 in larval zebrafish the next day (~ 60 hpf), and as described above for looping and ballooning, is
648 also dependent on both ventricular contractility and fluid forces derived from blood flow
649 (Peshkovsky et al., 2011; Staudt et al., 2014). Cardiomyocytes residing in the original, singular
650 outer layer of the ventricle wall extend protrusions toward the interior, then leave the outer layer,
651 migrating and proliferating as the trabeculae mature and project across the chamber. This process
652 requires Notch1, which signals to the endocardium to produce Neuregulin2a and activate the
653 epidermal growth factor (EGF) receptor family member Erbb2/4 in cardiomyocytes (Jimenez-
654 Amilburu et al., 2016; Peshkovsky et al., 2011; Rasouli and Stainier, 2017; Samsa et al., 2015).
655 In addition, several other EGF-like ligands are expressed during trabeculation, including *hbegfa*
656 (Samsa et al., 2016). The spacing of trabeculae is determined in part by the migration and
657 insertion of neural crest-derived cardiomyocytes into the initial ventricular wall, which
658 subsequently express the Notch ligand Jag2b and signal to adjacent cells (Abdul-Wajid et al.,
659 2018). Cardiac contraction and blood flow induce *notch1* expression in endocardial cells (Samsa
660 et al., 2015), and ventricular cardiomyocytes respond to Notch signaling only after the normal
661 degradation of the cardiac jelly that lies between the endocardial cells and cardiomyocytes (Del
662 Monte-Nieto et al., 2018; Rasouli and Stainier, 2017). Furthermore, Notch signaling in
663 ventricular cardiomyocytes is activated by chamber contraction not long after establishment of
664 the regular heartbeat (~ 28 hpf in zebrafish) (Samsa et al., 2015). Thus, a transient oil-induced
665 impact on cardiac contractility at the midpoint of cardiogenesis, as in the exposures here, could
666 also disrupt trabeculation in the post-hatch ventricle by reducing or delaying Notch signaling.

667 Consistent with this, the ventricular cardiac jelly layer did not degrade in oil-exposed herring
668 larvae, and there was a corresponding accumulation of disorganized ventricular cardiomyocyte
669 aggregations ("caps") at hatch. Therefore, the abnormal persistence of visible cardiac jelly is
670 likely a novel and predictive endpoint for subsequent defects in trabeculation.
671 Embryonic oil exposure led to two separate and concentration-dependent effects on
672 trabeculation in herring larvae. Specifically, the medium (140 ng/g) exposure increased the initial
673 spacing of trabeculae and produced abnormal rounded aggregations of myosin heavy chain
674 immunofluorescence. While the low treatment (64 ng/g) only affected myosin distribution, these
675 fish survived and yet showed an increased trabecular density (hypertrophy) later on. The co-
676 localization of the myosin heavy chain aggregates with nuclei suggests that these may represent
677 proliferative cardiomyocytes. As cardiomyocytes divide during trabeculation in zebrafish, they
678 become rounder, disassemble sarcomeres, and lose striated myofibrils before mitosis. A minimal
679 pool of sarcomeres remains intact only at the rounded cell periphery, then myofibrils reassemble
680 fully after division when subsequent daughter cells elongate (Uribe et al., 2018). The spherical
681 forms observed here with myosin heavy chain antibody were likely recently divided (or dividing)
682 cardiomyocytes, suggesting that transient embryonic crude oil toxicity induces an early (and
683 basal) hyperproliferative response during larval trabeculation. Later determinants of
684 trabeculation in zebrafish or other species are not yet known. However, our findings here for 67
685 dpf fish suggest that cardiomyocyte proliferation continues throughout the extent of the
686 trabeculae in the maturing heart. Although we were unable to quantify individual cardiomyocyte
687 density, the hypertrophy of the ventricle at 125 dpf is likely attributable to a relative increase in
688 cell number and size. This would be consistent with previous observations of ventricular
689 hypercellularity in oil-exposed pink salmon (Incardona et al., 2015), as well as an important

690 recent discovery in zebrafish showing that loss of normal Notch1-mediated trabecular spacing in
691 embryos causes pathological hypertrophy and reduced swimming performance in surviving
692 adults (Abdul-Wajid et al., 2018). We therefore recommend that future studies of delayed oil
693 toxicity in fish focus on pharmacological and biophysical-based disruptions of the genetic
694 pathways that underpin trabeculation in the larval and juvenile heart.
695 The modification of the internal structure of the spongy myocardium provides an additional,
696 novel clue into the longstanding puzzle of why zebrafish (Hicken et al., 2011) and herring and
697 pink salmon (Incardona et al., 2015) exposed to trace concentrations of crude oil relatively
698 briefly during embryogenesis nevertheless show a reduction in cardiorespiratory performance
699 that persists into much later stages of life – i.e., after many months of normal feeding and growth
700 in clean water. In adult fish, organ-level gross morphometry initially implicated a rounder
701 ventricle shape in reduced cardiac output and swimming performance found naturally (Claireaux
702 et al., 2005), or as a consequence of embryonic oil exposure (Hicken et al., 2011). While the
703 structure of the compact myocardium was not assessed in oil-exposed fully mature, adult
704 zebrafish (11 months post-exposure) (Hicken et al., 2011), embryonic oil exposure in pink
705 salmon led to a thinning of the juvenile compact myocardium (8- to 10-months post-exposure),
706 and both pink salmon and herring juveniles showed elongated rather than rounded ventricles
707 (i.e., increased aspect ratio) (Incardona et al., 2015). The determinants of ventricular shape in
708 juvenile herring or salmon are unclear, nor is the relationship between ventricular shape and
709 cardiac output. However, luminal volume and the density of trabeculation are likely to more
710 consistently influence cardiac output at earlier juvenile stages when the compact myocardium
711 consists of only a single layer of cardiomyocytes and has not begun to proliferate. Notably, at the
712 stages studied here (125 dpf, ~ 4 months post-exposure), the compact myocardium had not yet

713 begun to proliferate and was still only a single layer of cardiomyocytes, but we still observed a
714 similar elongation of the ventricle as observed in 10-month old oil-exposed fish with a
715 multicellular compact myocardium (Incardona et al., 2015). Intriguingly, controls showed an
716 inverse relationship between condition factor and ventricular aspect ratio, while oil-exposed fish
717 showed no relationship. Therefore, embryonic oil exposure overrides the normal factors
718 controlling ventricular shape in juveniles. It is possible that the hypertrophic response we
719 observed here in the early juvenile spongy myocardium leads to elongation of the ventricle,
720 which left unabated, could continue on to produce a terminally rounded ventricle in fully adult,
721 near-senescent fish. Additional studies should focus on how this crude oil injury phenotype
722 ultimately impacts individual survival.
723 From the perspective of assessing losses of culturally, ecologically, and commercially
724 important fishes, it would be advantageous to identify molecular markers for normal and
725 pathophysiological heart development in species that spawn in clean and contaminated
726 environments, respectively. Such biological indicators (or molecular initiating events) could
727 meet a wide array of resource management needs, including field-based determinations of injury
728 in habitats degraded by PACs originating from oil spills, urban stormwater runoff, and legacy
729 sediment pollution. To this end, we focused here on quantification of gene expression using real-
730 time PCR. QPCR is suitable for the sample sizes typical of fish early life history stages, rapidly
731 adaptable across multiple species, and offers a platform that is potentially adaptable to remote
732 sensing in future field studies. Nevertheless, there remain a few key challenges to this approach.
733 The first is the need to accurately measure tissue-specific changes in gene expression against a
734 backdrop of mRNA extracted from whole animals. This signal-to-noise problem is particularly
735 important for oil-responsive genes that are expressed at a relatively low level but have an

736 outsized influence on embryolarval development (Sørhus et al., 2016a; Sørhus et al., 2017).
737 Some of these genes are known to be cardiac-specific or expressed only in the heart at the
738 embryonic stages studied here, while others have broader expression patterns in multiple
739 embryonic structures. The second is the challenge of gene annotation and isoform identification
740 in non-model species, with or without a sequenced genome. Target genes can be selected using a
741 hypothesis-driven approach based on anchoring to a well-defined injury phenotype (Edmunds et
742 al., 2015; Sørhus et al., 2016b) or, as we have done here, chosen based on the results of
743 transcriptome sequencing in other species (Sørhus et al., 2017; Xu et al., 2016). A final
744 challenge relating to this approach is that many of these target genes, especially those expressed
745 only in the developing heart, are very low abundance transcripts. The variability inherent in
746 measuring low abundance genes creates a demand for higher statistical power, which itself often
747 conflicts with what is logistically feasible for sampling strategies with fish embryos and larvae.
748 Recognizing the above limitations, we assessed the expression of genes encoding the major
749 $Ca^{2+}$-handling proteins in cardiomyocytes. These included the SR $Ca^{2+}$ release channel
750 (ryanodine receptor isoform 2; *ryr2*), the SR $Ca^{2+}$ uptake pump (SERCA2; *atp2a2*), and the
751 plasma membrane $Na^{+}/Ca^{2+}$ exchanger (NCX1; *nac1/2/4*). In embryos and early larvae of other
752 species, one or more of these genes were down-regulated in response to controlled crude oil
753 exposures (Sørhus et al., 2017; Sørhus et al., 2016b; Xu et al., 2016). This includes an Atlantic
754 haddock contig originally identified as *nac1* but most closely related to a herring *nac2* isoform
755 (as determined via a BLAST search) that was expressed in both juvenile heart and skeletal
756 muscle. While neither *nac2* nor *ryr* expression was altered significantly in the experiments
757 described, *atp2a2* was transiently down-regulated very early during exposure and at roughly the
758 same developmental stage as previously reported for Atlantic haddock (Sørhus et al., 2017).

By convention, distinct morphogenetic phenotypes serve to anchor the interpretation of changing gene expression patterns. For example, severe heart malformations in haddock at hatching (prior to ventricular ballooning) were preceded by the strong up-regulation of the $Ca^{2+}$-regulated cardiac morphogen bone morphogenetic protein 10 (*bmp10*) (Sørhus et al., 2017; Sørhus et al., 2016b) and subsequent upregulation of *nkx2.5*, a downstream, positive target of *bmp10*. However, in mahi mahi (Edmunds et al., 2015) and Pacific herring (present study) hatching with milder malformations, *nkx2.5* as well as *myl7* and *myh7* were down-regulated. The down-regulation of these three genes is therefore consistent with (or indicative of) the more nuanced crude oil cardiotoxicity phenotypes of reduced contractility (during exposure) and reduced size of the ventricle (after exposure) at hatch. Among the known roles for *nkx2.5* in vertebrate heart development, the gene in zebrafish specifies the binary fate of cardiomyocyte precursors into atrium- and ventricle-specific subtypes, with reduced *nkx2.5* function leading to a smaller ventricle (Targoff et al., 2013). While we did not quantify the number of atrial cardiomyocytes as a potential mechanism, the enlarged atria and the smaller ventricles observed here may be a consequence of an oil-induced down-regulation of *nkx2.5*.

Finally, we examined the expression of *notch1*, *nrg2*, and *hbegfa*, candidate genes with known or potential roles in zebrafish ventricular trabeculation. In zebrafish, all three are expressed in multiple embryonic tissues external to the heart, creating a challenge for interpreting gene expression levels from whole-embryo total mRNA. Of these, for example, *notch1* has the broadest expression, with high levels in the developing central nervous system (Thisse and Thisse, 2005). Read-count data in Atlantic haddock embryos provides the ability to link whole-embryo mRNA levels to expression patterns characterized by in situ hybridization (Sørhus et al., 2016a; Sørhus et al., 2017). In this case, genes that show cardiac-specific

782 expression by in situ hybridization had read counts that averaged about 90, while those with
783 broader expression, for example throughout the somites or neural tube, had read counts of ~
784 2000 – 9000. In Atlantic haddock embryos, which are similar in size to Pacific herring, read
785 counts for mRNAs of *notch1*, *nrg2* and *hbegf* were in the range of 2000 – 12,000, ~ 100, and 20
786 – 50, respectively. Thus, the oil-induced effects on expression of *nrg2* and *hbegfa* are likely to
787 reflect changes linked to the ventricular phenotype, while changes in cardiac *notch1* expression
788 might not be resolved against such a large pool of extracardiac mRNA. Because of this broad
789 expression, a negative result with *notch1* is equivocal, and the role of cardiac *notch1* expression
790 in abnormal heart form and function in response to oil exposure will require further study. The
791 effects of oil on the other putative trabeculation genes in herring embryos were stage-specific,
792 including both early down-regulation (*hbegfa*) and late up-regulation (*nrg2*), the latter possibly
793 as a consequence of over-compensation as tissue PAC concentrations declined and cardiac
794 function was restored. Future confirmation of gene expression at a cellular level via in situ
795 hybridization will further elucidate mechanisms of dysregulated ventricular trabeculation.
796 Nevertheless, these findings represent an important step in the development of new biomarkers
797 for delayed and persistent cardiotoxicity in response to low-level oil exposure.
798 In summary, these results expand our understanding of how acute, transient, and sublethal
799 crude oil toxicity in fish embryos produces a latent pathological remodeling of the post-hatching
800 heart, thereby reducing cardiorespiratory performance in surviving juveniles. The tissue doses
801 measured here, when normalized to lipids, overlap with previous studies showing impacts on
802 ventricular structure and function delayed even further in time in both Pacific herring and pink
803 salmon (Incardona et al., 2015). This is consistent with an adverse outcome pathway for crude oil
804 toxicity in fish that extends from the disruption of excitation-contraction coupling within

805 embryonic cardiomyocytes to defective trabeculation to pathological hypertrophy at the scale of
806 the maturing organ (Fig. 8). We have identified potential molecular indicators for key events in
807 this pathway, in the form of genes functioning in cardiac contractility (*atp2a2*, *myl7*, *myh7*),
808 ventricular cardiomyocyte specification (*nkx2.5*) and trabeculation (*nrg2*, *hbegfa*). Promisingly,
809 for example, the down-regulation of *myl7* and *myh7* genes is consistently associated with
810 contractility defects across several fish species. Finally, the delayed heart malformations
811 observed here would likely be sufficient to explain the reduced marine survival of pink salmon in
812 previous mark and recapture studies (Heintz, 2007; Heintz et al., 2000) . It is notable, however,
813 that these cardiac defects were evident in herring under controlled aquaculture conditions. In
814 natural habitats, the confluence of crude oil cardiotoxicity and other environmental co-stressors
815 such as thermal variation, predation, and pathogen exposures would likely further reduce
816 individual survival and, by extension, recruitment to populations that support humans and
817 aquatic ecosystems.
818
819 **References**
820
821 Abdul-Wajid, S., Demarest, B.L., Yost, H.J., 2018. Loss of embryonic neural crest derived
822 cardiomyocytes causes adult onset hypertrophic cardiomyopathy in zebrafish. Nat. Commun. 9,
823 4603.
824
825 Adeyemo, O.K., Kroll, K.J., Denslow, N.D., 2015. Developmental abnormalities and differential
826 expression of genes induced in oil and dispersant exposed Menidia beryllina embryos. Aquat.
827 Toxicol. 168, 60-71.
828

829 Andrés-Delgado, L., Mercader, N., 2016. Interplay between cardiac function and heart
830 development. Biochim. Biophys. Acta 1863, 1707-1716.
831
832 Arnaout, R., Ferrer, T., Huisken, J., Spitzer, K., Stainier, D.Y., Tristani-Firouzi, M., Chi, N.C.,
833 2007. Zebrafish model for human long QT syndrome. Proc. Natl. Acad. Sci. U. S. A. 104,
834 11316-11321.
835
836 Auman, H.J., Coleman, H., Riley, H.E., Olale, F., Tsai, H.J., Yelon, D., 2007. Functional
837 modulation of cardiac form through regionally confined cell shape changes. PLoS Biol. 5, e53.
838
839 Berdougo, E., Coleman, H., Lee, D.H., Stainier, D.Y., Yelon, D., 2003. Mutation of *weak*
840 *atrium/atrial myosin heavy chain* disrupts atrial function and influences ventricular
841 morphogenesis in zebrafish. Development 130, 6121-6129.
842
843 Brette, F., Machado, B., Cros, C., Incardona, J.P., Scholz, N.L., Block, B.A., 2014. Crude oil
844 impairs cardiac excitation-contraction coupling in fish. Science 343, 772-776.
845
846 Brette, F., Shiels, H.A., Galli, G.L.J., Cros, C., Incardona, J.P., Scholz, N.L., Block, B.A., 2017.
847 A Novel Cardiotoxic Mechanism for a Pervasive Global Pollutant. Sci. Rep. 7, 41476.
848
849 Carls, M.G., Rice, S.D., Hose, J.E., 1999. Sensitivity of fish embryos to weathered crude oil: Part
850 I. Low-level exposure during incubation causes malformations, genetic damage, and mortality in
851 larval Pacific herring (*Clupea pallasi*). Environ. Toxicol. Chem. 18, 481-493.

852

853 Claireaux, G., McKenzie, D.J., Genge, A.G., Chatelier, A., Aubin, J., Farrell, A.P., 2005.
854 Linking swimming performance, cardiac pumping ability and cardiac anatomy in rainbow trout.
855 J. Exp. Biol. 208, 1775-1784.
856
857 Del Monte-Nieto, G., Ramialison, M., Adam, A.A.S., Wu, B., Aharonov, A., D'Uva, G., Bourke,
858 L.M., Pitulescu, M.E., Chen, H., de la Pompa, J.L., Shou, W., Adams, R.H., Harten, S.K.,
859 Tzahor, E., Zhou, B., Harvey, R.P., 2018. Control of cardiac jelly dynamics by NOTCH1 and
860 NRG1 defines the building plan for trabeculation. Nature 557, 439-445.
861
862 Dietrich, A.C., Lombardo, V.A., Veerkamp, J., Priller, F., Abdelilah-Seyfried, S., 2014. Blood
863 flow and Bmp signaling control endocardial chamber morphogenesis. Dev. Cell 30, 367-377.
864
865 Ebert, A.M., Hume, G.L., Warren, K.S., Cook, N.P., Burns, C.G., Mohideen, M.A., Siegal, G.,
866 Yelon, D., Fishman, M.C., Garrity, D.M., 2005. Calcium extrusion is critical for cardiac
867 morphogenesis and rhythm in embryonic zebrafish hearts. Proc. Natl. Acad. Sci. U. S. A. 102,
868 17705-17710.
869
870 Edmunds, R.C., Gill, J.A., Baldwin, D.H., Linbo, T.L., French, B.L., Brown, T.L., Esbaugh,
871 A.J., Mager, E.M., Stieglitz, J.D., Hoenig, R., Benetti, D.D., Grosell, M., Scholz, N.L.,
872 Incardona, J.P., 2015. Corresponding morphological and molecular indicators of crude oil
873 toxicity to the developing hearts of mahi mahi. Sci. Rep. 5, 17326.
874

875 Esbaugh, A.J., Mager, E.M., Stieglitz, J.D., Hoenig, R., Linbo, T.L., Lay, C., Forth, H., Brown,
876 T.L., French, B.L., Scholz, N.L., Incardona, J.P., Morris, J.M., Benetti, D.D., Grosell, M., 2016.
877 The effects of weathering and chemical dispersion on Deepwater Horizon crude oil toxicity to
878 mahi-mahi (*Coryphaena hippurus*) early life stages. Sci. Total Environ. 543, 644-651.
879
880 Gardner, L.D., Peck, K.A., Goetz, G.W., Linbo, T.L., Cameron, J., Scholz, N.L., Block, B.A.,
881 Incardona, J.P., 2019. Cardiac remodeling in response to embryonic crude oil exposure involves
882 unconventional NKX family members and innate immunity genes. J. Exp. Biol. 222, jeb205567.
883
884 Glickman, N.S., Yelon, D., 2002. Cardiac development in zebrafish: coordination of form and
885 function. Semin. Cell Dev. Biol. 13, 507-513.
886
887 Griffin, F.J., Pillai, M.C., Vines, C.A., Kaaria, J., Hibbard-Robbins, T., Yanagimachi, R., Cherr,
888 G.N., 1998. Effects of salinity on sperm motility, fertilization, and development in the Pacific
889 herring, Clupea pallasi. Biol. Bull. 194, 25-35.
890
891 Gupta, V., Poss, K.D., 2012. Clonally dominant cardiomyocytes direct heart morphogenesis.
892 Nature 484, 479-484.
893
894 Hale, R., Strutt, D., 2015. Conservation of Planar Polarity Pathway Function Across the Animal
895 Kingdom. Annu. Rev. Genet. 49, 529-551.
896

Hatlen, K., Sloan, C.A., Burrows, D.G., Collier, T.K., Scholz, N.L., Incardona, J.P., 2010. Natural sunlight and residual fuel oils are an acutely lethal combination for fish embryos. Aquat. Toxicol. 99, 56-64.

Heintz, R.A., 2007. Chronic Exposure to Polynuclear Aromatic Hydrocarbons in Natal Habitats Leads to Decreased Equilibrium Size, Growth, and Stability of Pink Salmon Populations. Integr. Environ. Assess. Manag. 3, 351-363.

Heintz, R.A., Rice, S.D., Wertheimer, A.C., Bradshaw, R.F., Thrower, F.P., Joyce, J.E., Short, J.W., 2000. Delayed effects on growth and marine survival of pink salmon *Oncorhynchus gorbuscha* after exposure to crude oil during embryonic development. Mar. Ecol. Prog. Ser. 208, 205-216.

Hicken, C.E., Linbo, T.L., Baldwin, D.H., Willis, M.L., Myers, M.S., Holland, L., Larsen, M., Stekoll, M.S., Rice, G.S., Collier, T.K., Scholz, N.L., Incardona, J.P., 2011. Sub-lethal exposure to crude oil during embryonic development alters cardiac morphology and reduces aerobic capacity in adult fish. Proc. Natl. Acad. Sci. U. S. A. 108, 7086–7090.

Incardona, J.P., 2017. Molecular mechanisms of crude oil developmental toxicity in fish. Arch. Environ. Contam. Toxicol. 73, 19-32.

Incardona, J.P., Carls, M.G., Day, H.L., Sloan, C.A., Bolton, J.L., Collier, T.K., Scholz, N.L., 2009. Cardiac arrhythmia is the primary response of embryonic Pacific herring (Clupea pallasi) exposed to crude oil during weathering. Environ. Sci. Technol. 43, 201-207.

Incardona, J.P., Carls, M.G., Holland, L., Linbo, T.L., Baldwin, D.H., Myers, M.S., Peck, K.A., Rice, S.D., Scholz, N.L., 2015. Very low embryonic crude oil exposures cause lasting cardiac defects in salmon and herring. Sci. Rep. 5, 13499.

Incardona, J.P., Carls, M.G., Teraoka, H., Sloan, C.A., Collier, T.K., Scholz, N.L., 2005. Aryl hydrocarbon receptor-independent toxicity of weathered crude oil during fish development. Environ. Health Perspect. 113, 1755-1762.

Incardona, J.P., Collier, T.K., Scholz, N.L., 2004. Defects in cardiac function precede morphological abnormalities in fish embryos exposed to polycyclic aromatic hydrocarbons. Toxicol. Appl. Pharmacol. 196, 191-205.

Incardona, J.P., Gardner, L.D., Linbo, T.L., Brown, T.L., Esbaugh, A.J., Mager, E.M., Stieglitz, J.D., French, B.L., Labenia, J.S., Laetz, C.A., Tagal, M., Sloan, C.A., Elizur, A., Benetti, D.D., Grosell, M., Block, B.A., Scholz, N.L., 2014. Deepwater Horizon Crude Oil Impacts the Developing Hearts of Large Predatory Pelagic Fish. Proc. Natl. Acad. Sci. U. S. A. 111.

Incardona, J.P., Scholz, N.L., 2016. The influence of heart developmental anatomy on cardiotoxicity-based adverse outcome pathways in fish. Aquat. Toxicol. 177, 515-525.

941

942 Incardona, J.P., Scholz, N.L., 2018. Case study: the 2010 Deepwater Horizon oil spill, in:
943 Burggren, W., Dubansky, B. (Eds.), Development, Physiology, and Environment: A Synthesis.
944 Springer, London.

945

946 Incardona, J.P., Swarts, T.L., Edmunds, R.C., Linbo, T.L., Edmunds, R.C., Aquilina-Beck, A.,
947 Sloan, C.A., Gardner, L.D., Block, B.A., Scholz, N.L., 2013. Exxon Valdez to Deepwater
948 Horizon: comparable toxicity of both crude oils to fish early life stages. Aquat. Toxicol. 142-143,
949 303-316.

950

951 Incardona, J.P., Vines, C.A., Anulacion, B.F., Baldwin, D.H., Day, H.L., French, B.L., Labenia,
952 J.S., Linbo, T.L., Myers, M.S., Olson, O.P., Sloan, C.A., Sol, S., Griffin, F.J., Menard, K.,
953 Morgan, S.G., West, J.E., Collier, T.K., Ylitalo, G.M., Cherr, G.N., Scholz, N.L., 2012a.
954 Unexpectedly high mortality in Pacific herring embryos exposed to the 2007 Cosco Busan oil
955 spill in San Francisco Bay. Proc. Natl. Acad. Sci. U. S. A. 109, E51-58.

956

957 Incardona, J.P., Vines, C.A., Linbo, T.L., Myers, M.S., Sloan, C.A., Anulacion, B.F., Boyd, D.,
958 Collier, T.K., Morgan, S., Cherr, G.N., Scholz, N.L., 2012b. Potent phototoxicity of marine
959 bunker oil to translucent herring embryos after prolonged weathering. PLoS One 7, e30116.

960

961 Jimenez-Amilburu, V., Rasouli, S.J., Staudt, D.W., Nakajima, H., Chiba, A., Mochizuki, N.,
962 Stainier, D.Y.R., 2016. In Vivo Visualization of Cardiomyocyte Apicobasal Polarity Reveals

963 Epithelial to Mesenchymal-like Transition during Cardiac Trabeculation. Cell Rep. 17, 2687-
964 2699.
965
966 Jung, J.-H., Hicken, C.E., Boyd, D., Anulacion, B.F., Carls, M.G., Shim, W.J., Incardona, J.P.,
967 2013. Geologically distinct crude oils cause a common cardiotoxicity syndrome in developing
968 zebrafish. Chemosphere 91, 1146-1155.
969
970 Jung, J.H., Kim, M., Yim, U.H., Ha, S.Y., Shim, W.J., Chae, Y.S., Kim, H., Incardona, J.P.,
971 Linbo, T.L., Kwon, J.H., 2015. Differential Toxicokinetics Determines the Sensitivity of Two
972 Marine Embryonic Fish Exposed to Iranian Heavy Crude Oil. Environ. Sci. Technol. 49, 13639-
973 13648.
974
975 Jung, J.H., Lee, E.H., Choi, K.M., Yim, U.H., Ha, S.Y., An, J.G., Kim, M., 2017. Developmental
976 toxicity in flounder embryos exposed to crude oils derived from different geographical regions.
977 Comp. Biochem. Physiol. C-Pharmacol. Toxicol. Endocrinol. 196, 19-26.
978
979 Khursigara, A.J., Perrichon, P., Martinez Bautista, N., Burggren, W.W., Esbaugh, A.J., 2017.
980 Cardiac function and survival are affected by crude oil in larval red drum, *Sciaenops ocellatus*.
981 Sci. Total Environ. 579, 797-804.
982
983 Laurel, B.J., Copeman, L.A., Iseri, P., Spencer, M.L., Hutchinson, G., Nordtug, T., Donald, C.E.,
984 Meier, S., Allan, S.E., Boyd, D.T., Ylitalo, G.M., Cameron, J.R., French, B.L., Linbo, T.L.,

985 Scholz, N.L., Incardona, J.P., 2019. Embryonic crude oil exposure impairs growth and lipid
986 allocation in a keystone Arctic forage fish. iScience in press.
987
988 Li, X., Ding, G., Xiong, Y., Ma, X., Fan, Y., Xiong, D., 2018. Toxicity of Water-Accommodated
989 Fractions (WAF), Chemically Enhanced WAF (CEWAF) of Oman Crude Oil and Dispersant to
990 Early-Life Stages of Zebrafish (Danio rerio). Bull. Environ. Contam. Toxicol. 101, 314-319.
991
992 Linden, O., 1978. Biological effects of oil on early development of the Baltic herring *Clupea*
993 *harengus membras*. Mar. Biol. 45, 273-283.
994
995 Ljubojevic, S., Bers, D.M., 2015. Nuclear calcium in cardiac myocytes. J. Cardiovasc.
996 Pharmacol. 65, 211-217.
997
998 Madison, B.N., Hodson, P.V., Langlois, V.S., 2017. Cold Lake Blend diluted bitumen toxicity to
999 the early development of Japanese medaka. Environ. Pollut. 225, 579-586.
1000
1001 Martinez Barrio, A., Lamichhaney, S., Fan, G.C., Rafati, N., Pettersson, M., Zhang, H., Dainat,
1002 J., Ekman, D., Höppner, M., Jern, P., Martin, M., Nystedt, B., Liu, X., Chen, W., Liang, X., Shi,
1003 C., Fu, Y., Ma, K.C., Zhan, X., Feng, C., Gustafson, U., Rubin, C.-J., Sällman Almén, M., Blass,
1004 M., Casini, M., Folkvord, A., Laikre, L., Ryman, N., Ming-Yuen Lee, S., Xu, X., Andersson, L.,
1005 2016. The genetic basis for ecological adaptation of the Atlantic herring revealed by genome
1006 sequencing. eLife 5, e12081.
1007

1008 Marty, G.D., Hose, J.E., McGurk, M.D., Brown, E.D., Hinton, D.E., 1997. Histopathology and
1009 cytogenetic evaluation of Pacific herring larvae exposed to petroleum hydrocarbons in the
1010 laboratory or in Prince William Sound, Alaska, after the Exxon Valdez oil spill. Can. J. Fish.
1011 Aquat. Sci. 54, 1846-1857.
1012
1013 McCarty, L.S., Mackay, D., 1993. Enhancing ecotoxicological modeling and assessment. Body
1014 Residues and Modes Of Toxic Action. Environ. Sci. Technol. 27, 1718-1728.
1015
1016 McGuigan, K., Phillips, P.C., Postlethwait, J.H., 2004. Evolution of Sarcomeric Myosin Heavy
1017 Chain Genes: Evidence from Fish. Molec. Biol. Evol. 21, 1042-1056.
1018
1019 McKechnie, I., Lepofsky, D., Moss, M.L., Butler, V.L., Orchard, T.J., Coupland, G., Foster, F.,
1020 Caldwell, M., Lertzman, K., 2014. Archaeological data provide alternative hypotheses on Pacific
1021 herring (Clupea pallasii) distribution, abundance, and variability. Proceedings of the
1022 National Academy of Sciences 111, E807-E816.
1023
1024 Merks, A.M., Swinarski, M., Meyer, A.M., Müller, N.V., Özcan, I., Donat, S., Burger, A.,
1025 Gilbert, S., Mosimann, C., Abdelilah-Seyfried, S., Panáková, D., 2018. Planar cell polarity
1026 signalling coordinates heart tube remodelling through tissue-scale polarisation of actomyosin
1027 activity. Nat. Commun. 9, 2161.
1028
1029 Miquerol, L., Kelly, R.G., 2013. Organogenesis of the vertebrate heart. Wiley Interdisciplinary
1030 Reviews: Developmental Biology 2, 17-29.

Morris, J., Gielazyn, M., Krasnec, M., Takeshita, R., Forth, H., Labenia, J.S., Linbo, T.L., French, B.L., Gill, J.A., Baldwin, D.H., Scholz, N.L., Incardona, J.P., 2018. Crude oil cardiotoxicity to red drum embryos is independent of oil dispersion energy. Chemosphere 213, 205-214.

Nolan, T., Hands, R.E., Bustin, S.A., 2006. Quantification of mRNA using real-time RT-PCR. Nat. Protoc. 1, 1559-1582.

Panakova, D., Werdich, A.A., Macrae, C.A., 2010. Wnt11 patterns a myocardial electrical gradient through regulation of the L-type Ca(2+) channel. Nature 466, 874-878.

Peshkovsky, C., Totong, R., Yelon, D., 2011. Dependence of cardiac trabeculation on neuregulin signaling and blood flow in zebrafish. Dev. Dyn. 240, 446-456.

Pollino, C.A., Holdway, D.A., 2002. Toxicity testing of crude oil and related compounds using early life stages of the crimson-spotted rainbowfish (*Melanotaenia fluviatilis*). Ecotox. Environ. Safe. 52, 180-189.

Quiat, D., Voelker, K.A., Pei, J., Grishin, N.V., Grange, R.W., Bassel-Duby, R., Olson, E.N., 2011. Concerted regulation of myofiber-specific gene expression and muscle performance by the transcriptional repressor Sox6. Proc. Natl. Acad. Sci. U. S. A. 108, 10196-10201.

Raab, G., Klagsbrun, M., 1997. Heparin-binding EGF-like growth factor. Biochim. Biophys. Acta 1333, F179-199.

Raine, J.C., Turcotte, D., Tumber, V., Peru, K.M., Wang, Z., Yang, C., Headley, J.V., Parrott, J.L., 2017. The effect of oil sands tailings pond sediments on embryo-larval walleye (Sander vitreus). Environ. Pollut. 229, 798-809.

Rasouli, S.J., Stainier, D.Y.R., 2017. Regulation of cardiomyocyte behavior in zebrafish trabeculation by Neuregulin 2a signaling. Nat. Commun. 8, 15281.

Roberts, S.B., Hauser, L., Seeb, L.W., Seeb, J.E., 2012. Development of Genomic Resources for Pacific Herring through Targeted Transcriptome Pyrosequencing. PLOS ONE 7, e30908.

Rottbauer, W., Baker, K., Wo, Z.G., Mohideen, M.A., Cantiello, H.F., Fishman, M.C., 2001. Growth and function of the embryonic heart depend upon the cardiac-specific L-type calcium channel alpha1 subunit. Dev. Cell 1, 265-275.

Samsa, L.A., Givens, C., Tzima, E., Stainier, D.Y.R., Qian, L., Liu, J.D., 2015. Cardiac contraction activates endocardial Notch signaling to modulate chamber maturation in zebrafish. Development 142, 4080-4091.

Samsa, L.A., Ito, C.E., Brown, D.R., Qian, L., Liu, J., 2016. IgG-Containing Isoforms of Neuregulin-1 Are Dispensable for Cardiac Trabeculation in Zebrafish. PLoS One 11, e0166734.

Schmittgen, T.D., Livak, K.J., 2008. Analyzing real-time PCR data by the comparative C(T) method. Nat. Protoc. 3, 1101-1111o1108.

Sidhwani, P., Yelon, D., 2019. Fluid forces shape the embryonic heart: Insights from zebrafish. Curr. Top. Dev. Biol. 132, 395-416.

Sloan, C.A., Anulacion, B.F., Baugh, K.A., Bolton, J.L., Boyd, D., Boyer, R.H., Burrows, D.G., Herman, D.P., Pearce, R.W., Ylitalo, G.M., 2014. Northwest Fisheries Science Center's analyses of tissue, sediment, and water samples for organic contaminants by gas chromatography/mass spectrometry and analyses of tissue for lipid classes by thin layer chromatography/flame ionization detection NOAA Technical Memorandum, p. 61.

Somlyo, A.P., Somlyo, A.V., 2003. Ca2+ Sensitivity of Smooth Muscle and Nonmuscle Myosin II: Modulated by G Proteins, Kinases, and Myosin Phosphatase. Physiol. Rev. 83, 1325-1358.

Sørhus, E., Incardona, J.P., Furmanek, T., Jentoft, S., Meier, S., Edvardsen, R.B., 2016a. Developmental transcriptomics in Atlantic haddock: Illuminating pattern formation and organogenesis in non-model vertebrates. Dev. Biol. 411, 301-313.

Sørhus, E., Incardona, J.P., Furmanek, T., Scholz, N.L., Meier, S., Edvardsen, R.B., Jentoft, S., 2017. Novel adverse outcome pathways revealed by chemical genetics in a developing marine fish. eLife 6, e20707.

Sørhus, E., Incardona, J.P., Karlsen, Ø., Linbo, T.L., Sørensen, L., Nordtug, T., van der Meeren, T., Thorsen, A., Thorbjørnsen, M., Jentoft, S., Edvardsen, R.B., Meier, S., 2016b. Effects of crude oil on haddock reveal roles for intracellular calcium in craniofacial and cardiac development. Sci. Rep. 6, 31058.

Staudt, D., Stainier, D., 2012. Uncovering the molecular and cellular mechanisms of heart development using the zebrafish. Annu. Rev. Genet. 46, 397-418.

Staudt, D.W., Liu, J.D., Thorn, K.S., Stuurman, N., Liebling, M., Stainier, D.Y.R., 2014. High-resolution imaging of cardiomyocyte behavior reveals two distinct steps in ventricular trabeculation. Development 141, 585-593.

Steiness, E., Valentin, N., 1976. Myocardial digoxin uptake: dissociation between digitalis-induced inotropism and myocardial loss of potassium. Br. J. Pharmacol. 58, 183-188.

Targoff, K.L., Colombo, S., George, V., Schell, T., Kim, S.-H., Solnica-Krezel, L., Yelon, D., 2013. Nkx genes are essential for maintenance of ventricular identity. Development 140, 4203-4213.

Thisse, C., Thisse, B., 2005. High Throughput Expression Analysis of ZF-Models Consortium Clones, ZFIN Direct Data Submission.

1123 Uhler, A.D., Stout, S.A., Douglas, G.S., 2007. Chemical heterogeneity in modern marine
1124 residual fuel oils, in: Wang, Z., Stout, S.A. (Eds.), Oil Spill Environmental Forensics. Academic
1125 Press, London, pp. 327-348.
1126
1127 Uribe, V., Ramadass, R., Dogra, D., Rasouli, S.J., Gunawan, F., Nakajima, H., Chiba, A.,
1128 Reischauer, S., Mochizuki, N., Stainier, D.Y.R., 2018. In vivo analysis of cardiomyocyte
1129 proliferation during trabeculation. Development 145, dev164194.
1130
1131 Vehniäinen, E.R., Haverinen, J., Vornanen, M., 2019. Polycyclic Aromatic Hydrocarbons
1132 Phenanthrene and Retene Modify the Action Potential via Multiple Ion Currents in Rainbow
1133 Trout Oncorhynchus mykiss Cardiac Myocytes. Environ. Toxicol. Chem. 38, 2145-2153.
1134
1135 Wamhoff, B.R., Bowles, D.K., Owens, G.K., 2006. Excitation-transcription coupling in arterial
1136 smooth muscle. Circ. Res. 98, 868-878.
1137
1138 Wang, Z., Hollebone, B.P., Fingas, M., Fieldhouse, B., Sigouin, L., Landriault, M., Smith, P.,
1139 Noonan, J., Thouin, G., Weaver, J.W., 2003. Characteristics of spilled oils, fuels, and petroleum
1140 products: 1. Composition and properties of selected oils. U.S. Environmental Protection Agency,
1141 Washington, D.C.
1142
1143 Xie, F.L., Xiao, P., Chen, D.L., Xu, L., Zhang, B.H., 2012. miRDeepFinder: a miRNA analysis
1144 tool for deep sequencing of plant small RNAs. Plant Mol Biol 80, 75-84.
1145

1146 Xu, E.G., Mager, E.M., Grosell, M., Pasparakis, C., Schlenker, L.S., Stieglitz, J.D., Benetti, D.,
1147 Hazard, E.S., Courtney, S.M., Diamante, G., Freitas, J., Hardiman, G., Schlenk, D., 2016. Time-
1148 and Oil-Dependent Transcriptomic and Physiological Responses to Deepwater Horizon Oil in
1149 Mahi-Mahi (Coryphaena hippurus) Embryos and Larvae. Environ. Sci. Technol. 50, 7842-7851.
1150
1151 Yingzi, Y., Marek, M., 2015. Wnt-Frizzled/Planar Cell Polarity Signaling: Cellular Orientation
1152 by Facing the Wind (Wnt). Annu. Rev. Cell Dev. Biol. 31, 623-646.
1153
1154

1155
1156 **Acknowledgements**

1157 We thank Mary Arkoosh for use of wet and dry lab space at the Newport facility; Joe Dietrich
1158 for assistance with designing and building the exposure system and preparing growth tanks; Paul
1159 Iseri for small boat operations and herring fishing; Jana Labenia, David Baldwin, Jessica Lundin,
1160 and Julann Spromberg for assistance with exposures and sampling; and Paul Hershberger and
1161 Jake Gregg for providing juvenile herring for the comparative qPCR in heart and swimming
1162 muscle samples. We thank Julann Spromberg for her critical review of the manuscript. Funding
1163 was provided in part by the NOAA National Ocean Service, Office of Response and Restoration,
1164 Assessment and Restoration Division.

**Table 1: QPCR primers**

| Gene | Forward primer | Reverse primer | NCBI Reference Sequence | Efficiency (%) |
|---|---|---|---|---|
| **Reference genes** | | | | |
| *ef1a* | CTGGTATGGTTGTGACCTTCG | ACGGATATCCTTGACTGACACG | XM_012818387.1 | 105 |
| *mtm1* | CTCTGAAGCAGGAGGGTCAC | CTGACTGAGGAACGCAAACA | XM_012817813.1 | 113 |
| *rxrba* | ACCGATCTTCAGGCAAACAC | GGTACCTGAGCCATCGGTAA | XM_012833519.1 | 84 |
| *spop1* | TTTCAGTGCGATGTTTGAGC | GCTTTCCCCGTGTAGATGAA | XM_012825971.1 | 101 |
| *wdtc1* | GCTCTTCGCCAAGACAGATT | AGTTGTGGAAACGGATGGAG | XM_012838768.1 | 109 |
| **Target genes** | | | | |
| *atp2* | AGATCATCGAGTTCCTGCAGTC | CATGTTGTTGTAGATTGCCCGG | XM_012814918.1 | 112 |
| *cyp1a* | AGGAGCACATCAGCAAGGAG | ACCACCTGTCCGAACTCATC | XM_012831254.1 | 110 |
| *hbegfa* | TGGCAAACATCCGTAAACCTTC | TTTTCAACATCATAGGCACCCC | XM_012842112.1 | 100 |
| *nac2* | TGTCATTGGCTTCCTCACTGC | CCCTGCACATTCCAGTAGATAGC | XM_012828862.1 | 120 |
| *nkx2.5* | TGGATATTGTCAAGGAGGGGAAG | CTCGGGTGCAGACAAGTATTTCTG | XM_012831385.1 | 115 |
| *notch1* | TGGAGCCAACAAAGACATGC | GCTAGGAACAGGGGAGTCTC | XM_012830546.1 | 117 |

| | | | | |
|---|---|---|---|---|
| *myh7* | AGGGCTCCTCTTTCCAAACT | AAGCCCTTTCTGCAGATCCT | XM_012827835.1 | 108 |
| *myl7* | GAGGCTTTTGGTTGCATTGATC | TCATCCTTGTTGACGAATCCTG | XM_012831367.1 | 108 |
| *nrg2* | TCGTCCACTCATGCCCATTC | CGGACACATACCTTTCACTGTG | XM_012821330.1 | 116 |
| *ryr2* | GCTTGCTTGCAGTAGTGGTTTATC | GATGGCCAGCAGAATGACAATC | XM_012814530.1 | 137 |

1 **Table 2: PAC concentrations in water and Pacific herring embryo tissues**

| Oil load | Water Day 1 (µg/L) | Water Day 10 (µg/L) | Tissue Day 10 (ng/g wet weight) | Tissue Day 10 (ng/g lipid) |
|---|---|---|---|---|
| control | 0.070 ±0.002 | 0.014 ± 0.003 | 10.2 ± 0.9 | 619 ± 99 |
| 0.25 g/kg | 1.33 ± 0.13 | 0.26 ± 0.04 | 63.8 ± 10.3 | 3960 ± 723 |
| 0.5 g/kg | 1.85 ± 0.17 | 0.72 ± 0.16 | 140.3 ± 35.9 | 8025 ± 2104 |
| 1.0 g/kg | 4.15 ± 0.57 | 0.81 ± 0.02 | 237.5 ± 27.2 | 12879 ± 1486 |

2

3

**Table 3: Anatomical measurements in 125 dpf Pacific herring juveniles**

| Measure | Control (N = 9) | ∑PAC 64 ng/g (N = 18) | P value |
|---|---|---|---|
| length (mm) | 27.4 ± 1.6 | 27.9 ± 0.8 | 0.76 |
| wet weight (g) | 0.079 ± 0.021 | 0.089 ± 0.011 | 0.63 |
| K | 0.32 ± 0.02 | 0.39 ± 0.02 | 0.03 |
| ventricle lateral area ($mm^2$) | 0.81 ± 0.08 | 0.91 ± 0.08 | 0.4 |
| ventricle ventral area ($mm^2$) | 0.99 ± 0.10 | 1.04 ± 0.05 | 0.6 |
| ventricle lateral aspect ratio | 2.17 ± 0.05 | 1.91 ± 0.04 | 0.0002 |
| ventricle ventral aspect ratio | 1.86 ± 0.07 | 1.76 ± 0.03 | 0.15 |

**Table 4: Target gene expression levels in heart vs. skeletal muscle of juvenile Pacific herring**

| | Heart:skeletal muscle mean relative expression (N = 3) |
|---|---|
| *myl7* | 469,744 ± 198,257 |
| *nkx2.5* | 70,468 ± 30,091 |
| *nrg2* | 61 ± 25 |
| *ryr2* | 24 ± 11 |
| *atp2a2* | 7 ± 1 |
| *notch1* | 6 ± 2 |
| *nac2* | 1.3 ± 0.1 |
| *myh7* | 0.2 ± 0.1 |
| *hbegfa* | 0.2 ± 0.1 |

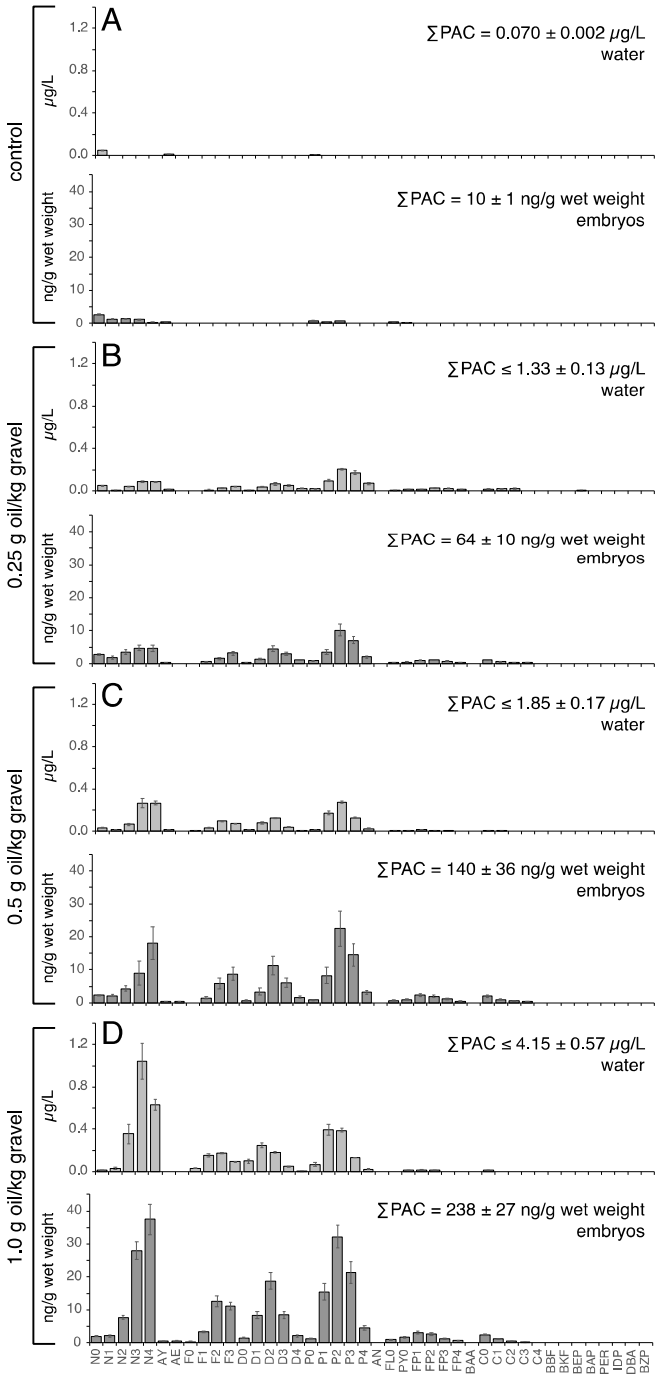
control
0.25 g oil/kg gravel
0.5 g oil/kg gravel
1.0 g oil/kg gravel
A
B
C
D
µg/L
ng/g wet weight
∑PAC = 0.070 ± 0.002 µg/L
water
∑PAC = 10 ± 1 ng/g wet weight
embryos
∑PAC ≤ 1.33 ± 0.13 µg/L
water
∑PAC = 64 ± 10 ng/g wet weight
embryos
∑PAC ≤ 1.85 ± 0.17 µg/L
water
∑PAC = 140 ± 36 ng/g wet weight
embryos
∑PAC ≤ 4.15 ± 0.57 µg/L
water
∑PAC = 238 ± 27 ng/g wet weight
embryos
N0 N1 N2 N3 N4 AY AE F0 F1 F2 F3 D0 D1 D2 D3 D4 P0 P1 P2 P3 P4 AN FL0 FL1 FP1 FP2 FP3 FP4 BAA C0 C1 C2 C3 C4 BBF BKF BEP BAP PER IDP DBA BZP

12

Figure 1. Effects of embryonic exposure on gross morphology of yolk sac larvae. (A – D) Representative images of yolk sac larvae at peak hatch. (A) control; (B) 64 ng/g (1.3 µg/L) dose; (C) 140 ng/g (1.9 µg/L) dose; (D) 238 ng/g (4.2 µg/L) dose. Scale bar (A) is 1 mm. (E) Relationship between tissue dose and incidence of pericardial edema scored as deformation of the anterior yolk mass. Data are mean ± s.e.m. (N = 4) for 30 larvae from each of 4 replicate exposures per dose. (F) Dry weights of embryos at end exposure (light gray bars) and larvae at hatch (dark gray bars) and 1-week post-hatch (white bars). Data are mean ± s.e.m. (N = 4) for each of 4 replicate pools of 50 embryos or larvae, normalized per individual.

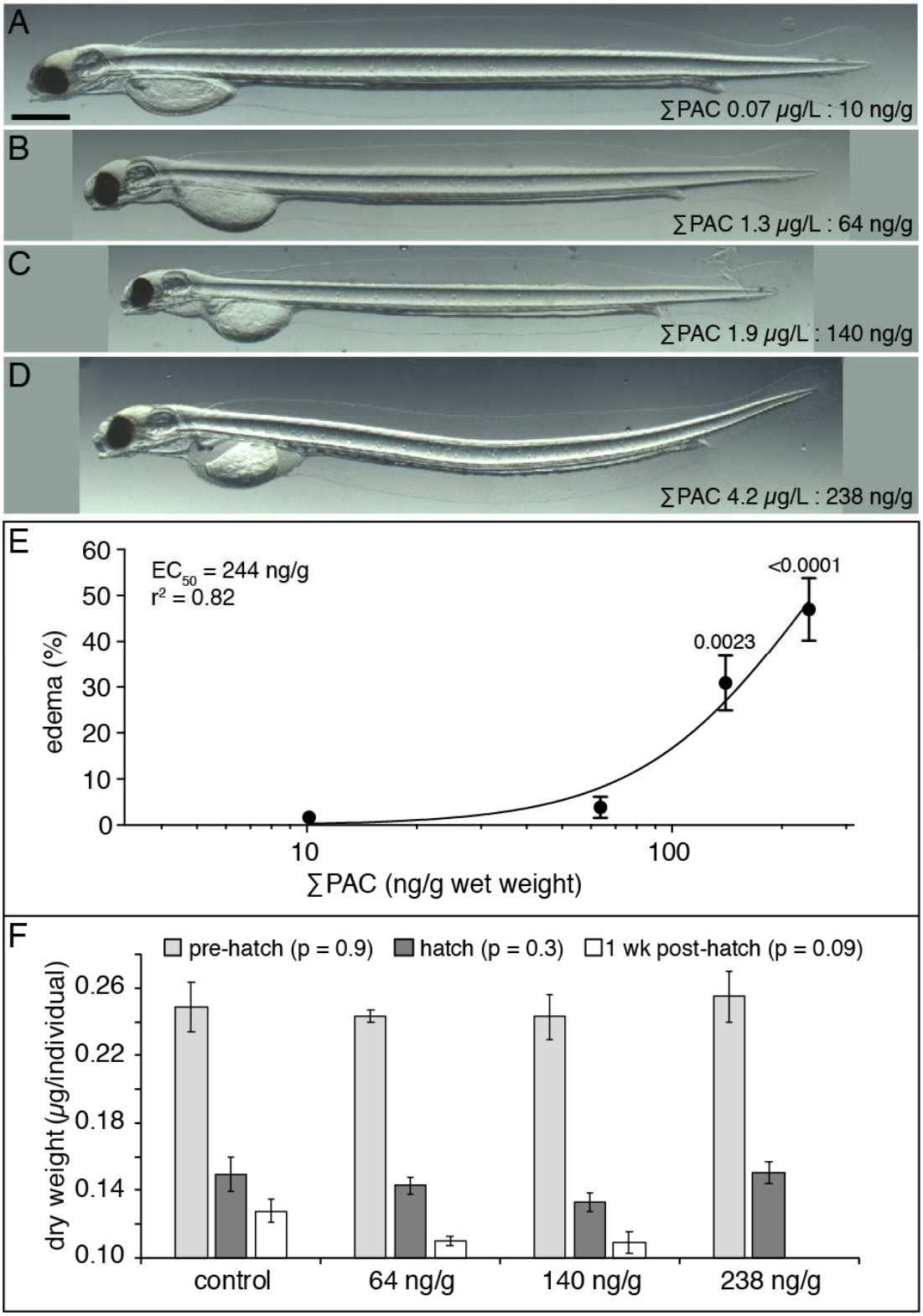
A
∑PAC 0.07 µg/L : 10 ng/g
B
∑PAC 1.3 µg/L : 64 ng/g
C
∑PAC 1.9 µg/L : 140 ng/g
D
∑PAC 4.2 µg/L : 238 ng/g
E
EC50 = 244 ng/g
r2 = 0.82
<0.0001
0.0023
edema (%)
60
50
40
30
20
10
0
10
100
∑PAC (ng/g wet weight)
F
pre-hatch (p = 0.9)
hatch (p = 0.3)
1 wk post-hatch (p = 0.09)
dry weight (µg/individual)
0.26
0.22
0.18
0.14
0.10
control
64 ng/g
140 ng/g
238 ng/g

21

Figure 2. Dose-dependent reduction in the degree of ventricular ballooning at hatch. High magnification lateral views of the heart are shown with anterior to the left, representing video frames taken from the end of ventricular diastole/atrial systole. The atrium is outlined by the dashed light magenta line, ventricle outlined by the orange dotted line. The solid white line traces the atrial endocardium. (A) 10 dpf control embryo, with white arrow indicting the ventricle outer curvature and white arrowhead indicating the inner curvature (behind atrium). Hatched yolk sac larvae shown for control (B), 64 ng/g dose (C), 140 ng/g dose (D) and 238 ng/g dose (E). Scale bar is 50 µm.

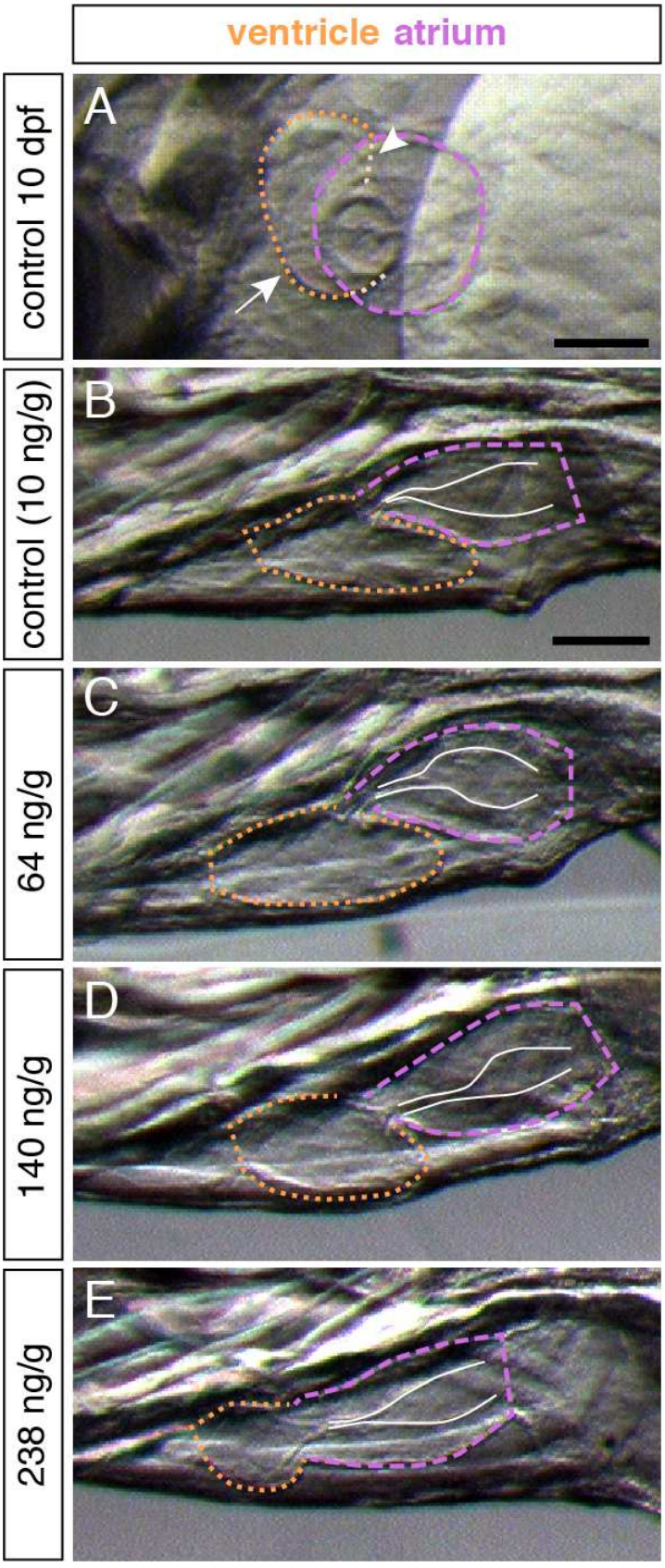
ventricle atrium
control 10 dpf
A
control (10 ng/g)
B
64 ng/g
C
140 ng/g
D
238 ng/g
E

30

Figure S3. Delayed initiation of ventricular ballooning in feeding stage larvae. For comparison, initial ventricular phenotype is shown at 1 dph for control (A) and the high 238 ng/g dose group (B). Identical view at 8 dph for control (C) and 238 ng/g dose (D). Ventricle (*v*) is outlined with the dashed yellow line. Atrium, *a*. White arrows indicate the cleithrum. Scale bars are 100 µm.

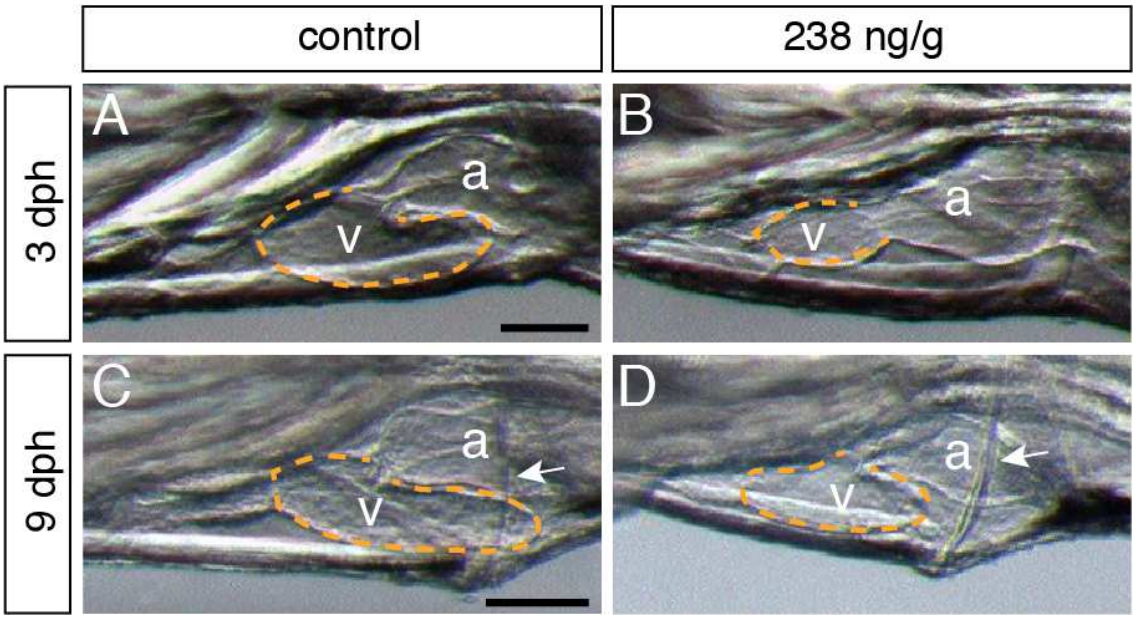

Figure 3. Dose-dependent increase in atrial and ventricular wall thickness at hatch. Representative high magnification views of the ventral atrial wall (A, B) and posterior ventricular wall (A', B') were taken from video frames at end diastole for both chambers. (A, A') control, (B, B') 238 ng/g dose. Dotted black brackets indicate region of thickness measurements. Arrows (A', B') indicates position of the atrioventricular junction for the ventricle. (C) Thickness of atrial and ventricular walls (μm) quantified for 10 larvae from each of 4 replicate exposures (mean ± s.e.m., N = 4). Asterisks indicate groups that are statistically different from control ($\alpha = 0.05$) by ANOVA and Dunnett post-hoc test. Scale bar (B') is 50 μm.

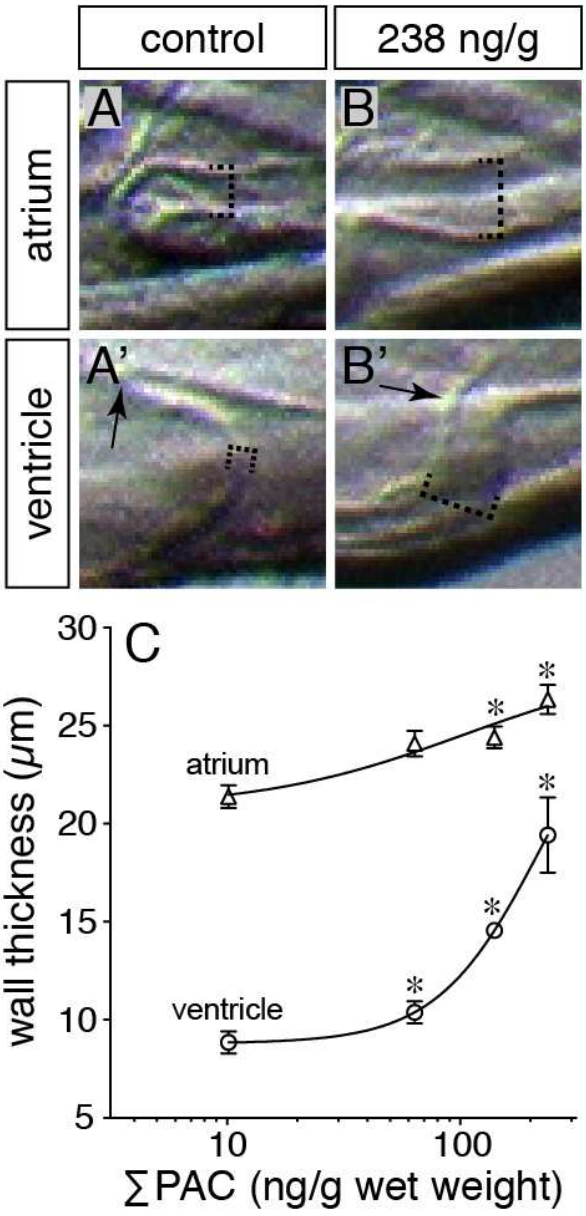
control
238 ng/g
atrium
ventricle
A
B
A'
B'
C
wall thickness (μm)
30
25
20
15
10
5
atrium
ventricle
*
10
100
∑PAC (ng/g wet weight)

45

46

47

Figure S4. Dose-dependent accumulation of cardiomyocyte aggregates on the posterior ventricle at hatch. (A, B) Light micrographs of hearts in live larvae, from video frames taken at ventricular end diastole in control (A) and 238 ng/g dose (B). White arrow indicates thickened "cap" on the posterior end of the ventricle (*v*). Atrium, *a*. (C) Incidence of ventricular cap across dose series. Data are mean ± s.e.m. (N = 4) of incidence among 30 larvae per 4 replicates at each dose. ANOVA for effect of oil exposure $p = 0.0025$; asterisk indicates dose level significantly different from control by Dunnett's post-hoc test. (D – F) Labeling of atrial (*a*) and ventricular (*v*) cardiomyocytes with anti-myosin heavy chain antibody identifies ventricular caps as cardiomyocyte aggregates. Images show anti-myosin antibody immunofluorescence (white signal) in lateral views similar to light micrographs in (A, B) for control (D) and two levels of severity for the ∑PAC 238 ng/g dose (E, F). Arrows indicate disorganized cardiomyocyte aggregates. Scale bar (D) is 50 µm.

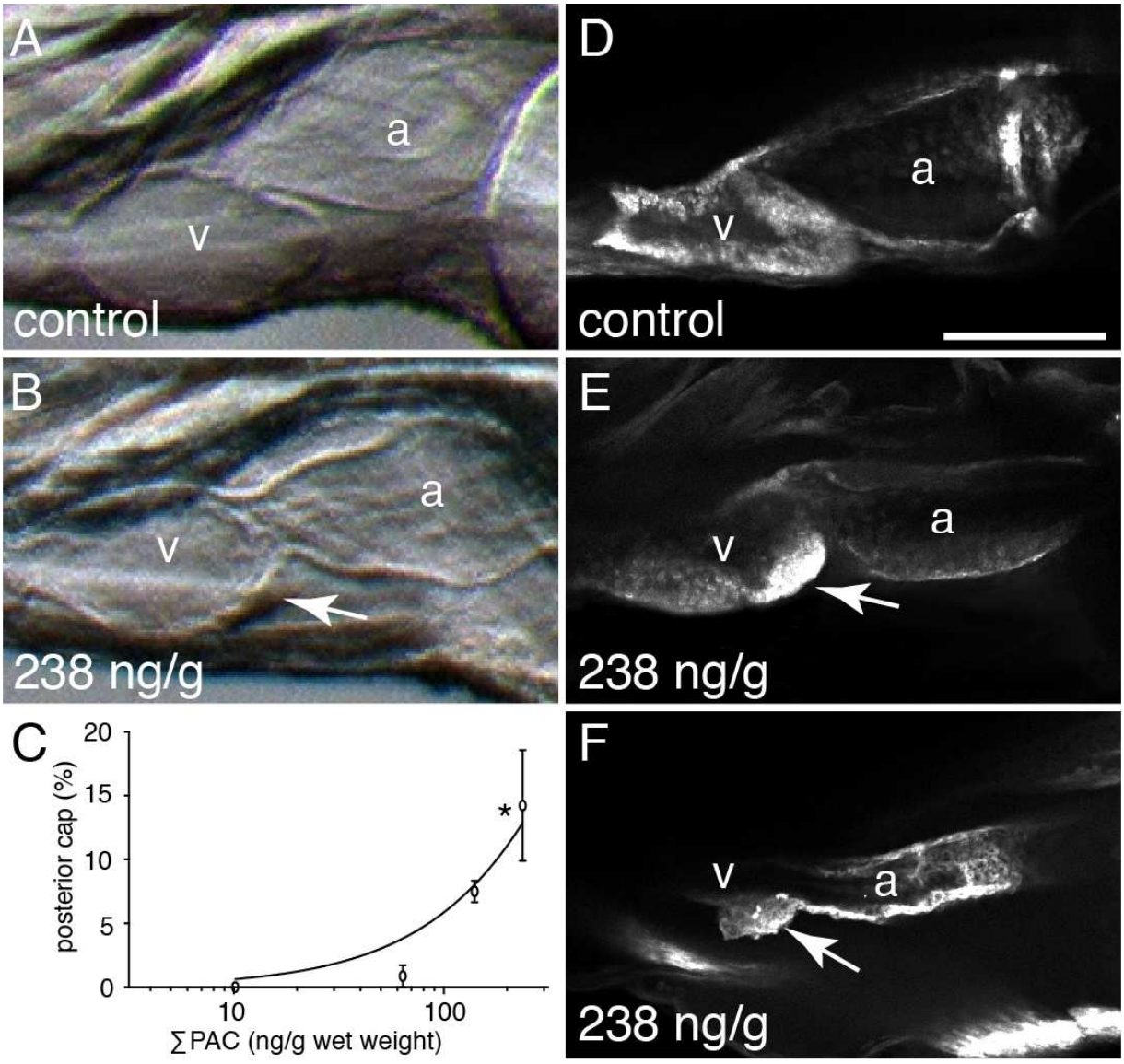
A
a
v
control
D
a
v
control
B
a
v
238 ng/g
E
a
v
238 ng/g
C
posterior cap (%)
20
15
10
5
0
*
10
100
∑PAC (ng/g wet weight)
F
v
a
238 ng/g

60

61

Figure 4. Quantification of dose-dependent effects of oil exposure on cardiac morphology and function at hatch. All data are mean ± s.e.m. (N = 4) from at least 23 larvae from each of 4 replicate exposures for each dose at 1 dph, plotted against internal ∑PAC dose with non-linear regression models as described in the Materials and Methods section. Significance compared to control after ANOVA and Dunnett's post-hoc test is indicated by p values (A, B, D) or asterisks (C). (A) Area of the posterior ventricle ($mm^2$). (B) Atrioventricular (AV) angle (degrees). (C) Chamber areas ($mm^2$) for atrium at end diastole (blue triangles) and end systole (light blue diamonds), and ventricle at end diastole (orange circles) and end systole (light orange squares). (D) Contractility measured as fractional shortening for the atrium (blue triangles) and ventricle (orange diamonds).

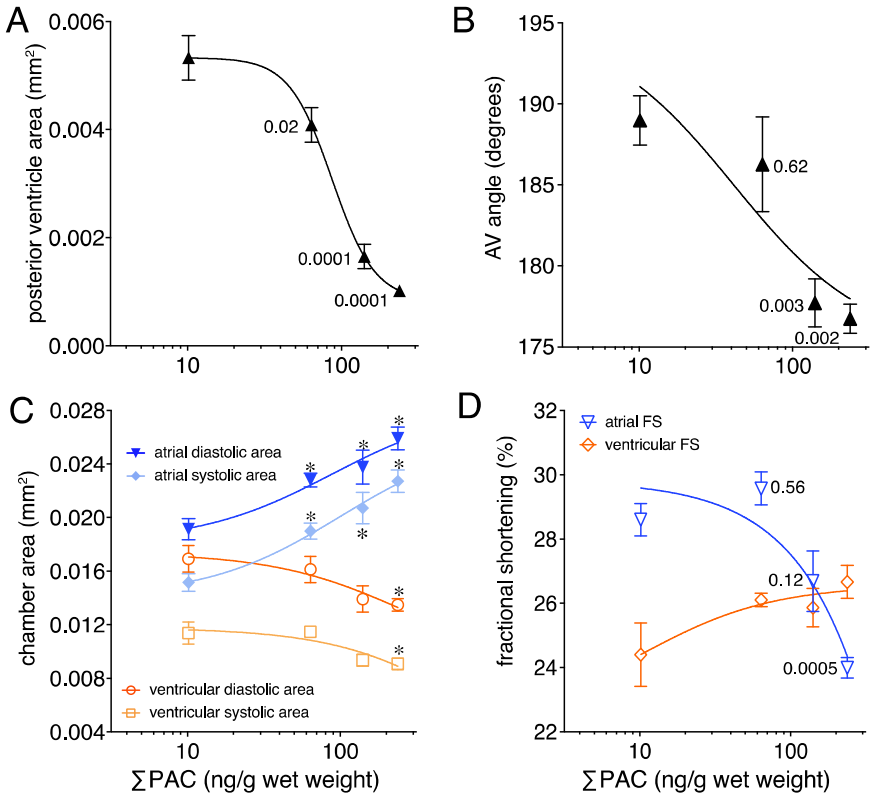
A
posterior ventricle area (mm²)
0.006
0.004
0.002
0.000
0.02
0.0001
0.0001
10
100
B
AV angle (degrees)
195
190
185
180
175
0.62
0.003
0.002
10
100
C
chamber area (mm²)
0.028
0.024
0.020
0.016
0.012
0.008
0.004
atrial diastolic area
atrial systolic area
ventricular diastolic area
ventricular systolic area
10
100
∑PAC (ng/g wet weight)
D
fractional shortening (%)
32
30
28
26
24
22
atrial FS
ventricular FS
0.56
0.12
0.0005
10
100
∑PAC (ng/g wet weight)

Figure 5. Abnormal trabeculation in larvae surviving to 67 dpf. (A, B) Representative live larvae at 67 dpf from control (A) and ∑PAC 140 ng/g dose groups (B). (C) Confocal images of cortical and trabecular cardiomyocytes labeled with anti-myosin heavy chain antibody, with control at top, ∑PAC 64 ng/g dose in the middle and 140 ng/g dose at bottom. Images were collected from the center of the ventral wall of the ventricle, with the ventral cortical layer at top and trabeculae extending downward to the interior of the ventricle. Quantification of trabecular spacing immediately near the cortical layer is shown plotted to the right of the representative images. Data are mean ± s.e.m. of 13-14 trabecular spaces in each of 5 or 4 individual larvae for control and each exposed dose, respectively. ANOVA was significant for effect of exposure ($p = 0.0025$) with the 140 ng/g dose different from control by Dunnett's post-hoc test ($p = 0.003$). (D, E) Cardiomyocyte myosin heavy chain distribution (D, E; red) relative to nuclei (D', E'; green) in confocal images taken from the ventral aspect of the ventricle for control (D-D") and ∑PAC 140 ng/g dose (E-E"). Merged images shown in (D", E"). Inset in each shows higher magnification view of individual cells from the same image; arrows indicate co-localization of nuclei with spheroid myosin heavy chain immunofluorescence. Scale bars are 2 mm (A), 10 µm (C) and 50 µm (E").

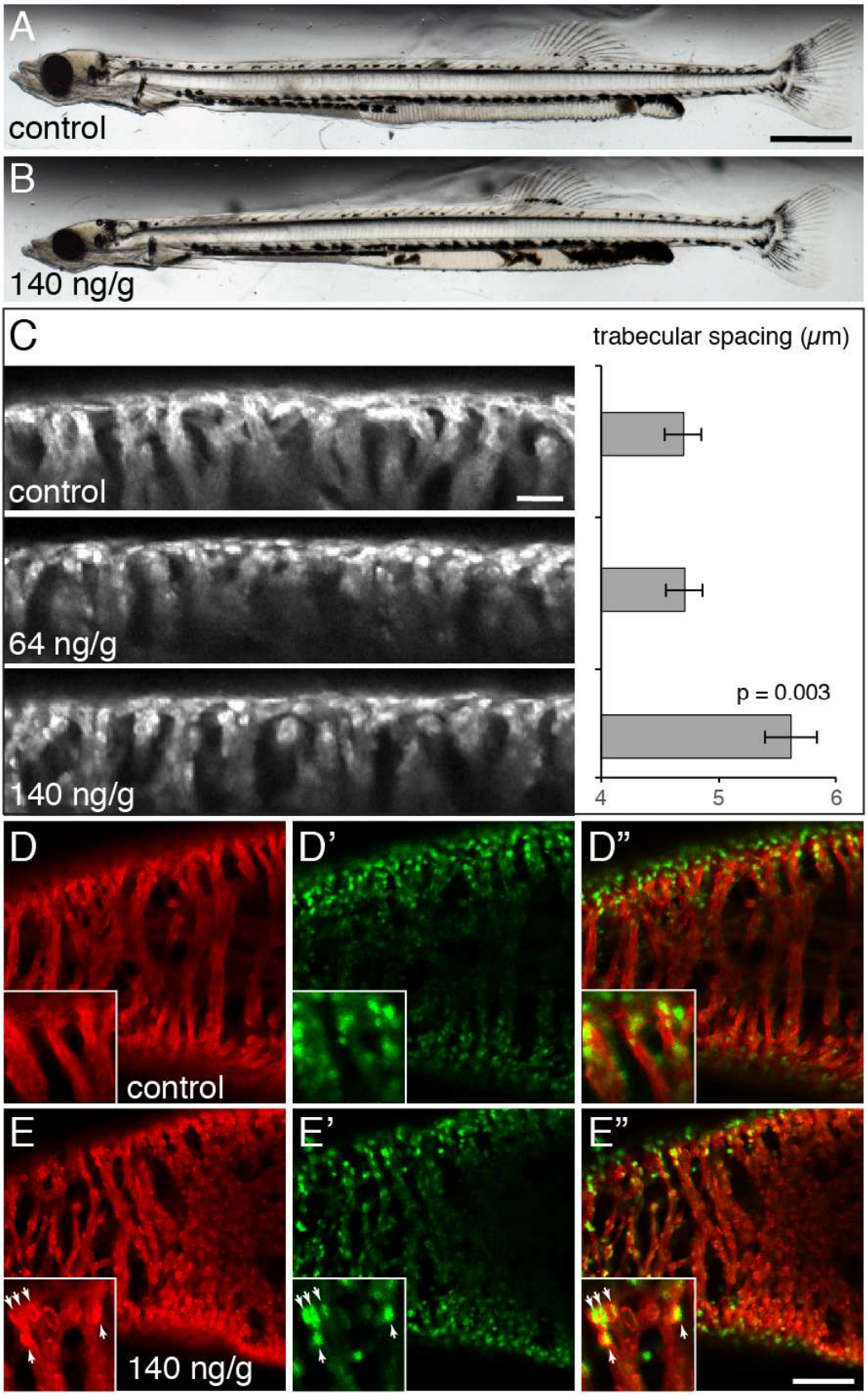
A
control
B
140 ng/g
C
trabecular spacing (μm)
control
64 ng/g
140 ng/g
p = 0.003
4
5
6
D
D'
D"
control
E
E'
E"
140 ng/g

89

Figure 6. Altered ventricular shape and hypertrophy of trabeculae in early juveniles at 125 dpf. Lateral views of freshly-dissected hearts from representative control (A) and 64 ng/g dose group (B). Anterior is to the left, dorsal at top. Ventricle, *v*; atrium, *a*; bulbus arteriosus, *ba*. Scale bar is 0.5 mm (A). (C) Linear regression model relating aspect ratio to condition factor K at 125 dpf in controls (N = 9; blue circles) and the 64 ng/g dose group (N = 15; black squares). Representative images of myosin heavy chain immunofluorescence in histological sections from a subset of 125 dpf hearts from control (D) and 64 ng/g dose group (E). Total cellularity (F, left plot) was quantified by counting DAPI-stained nuclei and normalizing to total pixel area occupied by myosin heavy chain labeling, while trabecular hypertrophy (F, right plot) was quantified as the percentage of pixels from myosin heavy chain labeling relative to total pixel area contained by the ventricle perimeter. Data represent mean ± s.e.m. of measurements from 2 to 3 replicate sections from each of 6 control hearts and 7 hearts from the 64 ng/g dose group. One-way nested ANOVA was significant for effect of treatment ($p = 0.04$) but not replicate ($p = 0.14$); post-hoc t-test showed a significant difference between control and exposed ($p = 0.04$).

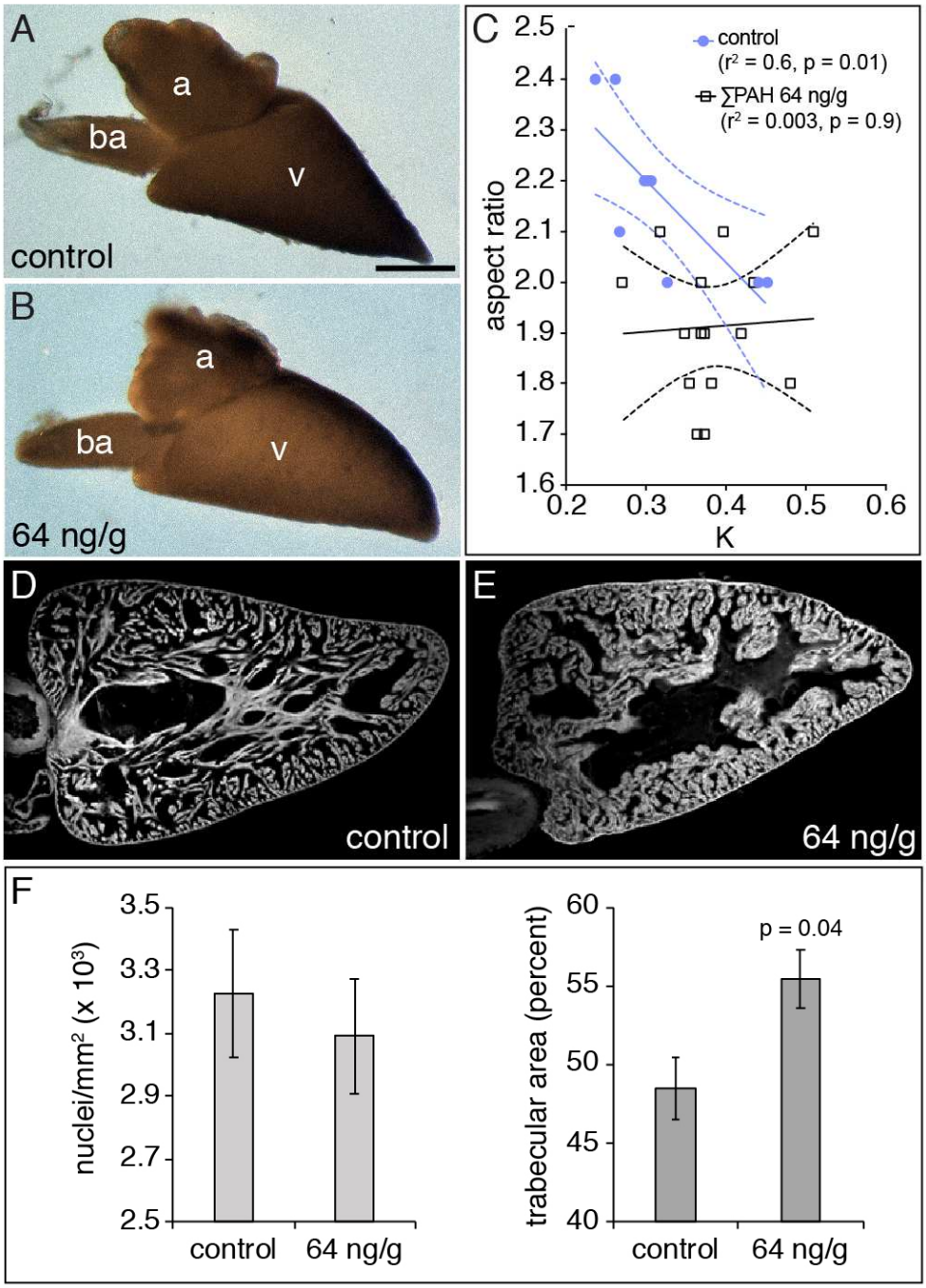
A
a
ba
v
control
B
a
ba
v
64 ng/g
C
control
(r² = 0.6, p = 0.01)
∑PAH 64 ng/g
(r² = 0.003, p = 0.9)
aspect ratio
K
D
control
E
64 ng/g
F
nuclei/mm² (x 10³)
control
64 ng/g
trabecular area (percent)
p = 0.04
control
64 ng/g

104

Figure 7. Quantification of expression levels of genes functioning in cardiac $Ca^{2+}$ handling, contractility, ventricular specification and trabeculation. As a reference for the exposure time course and PAC toxicokinetics, expression of *cyp1a* is shown in (A). Expression is shown for four time points; three during embryonic exposure (6 dpf, 8 dpf, 10 dpf) and one 3 days after exposure in yolk sac larvae (hatch). Dosing levels are color-coded, control (blue), 64 ng/g (yellow), 140 ng/g (orange) and 238 ng/g (black) tissue ∑PAC. For each gene, lines are plotted for each dose between each time point to highlight general trends. Data represent mean (N = 4) fold-change relative to controls normalized to the geometric mean of three reference genes (see Methods and Materials). For simplicity, error bars are omitted, but complete set of raw data and variability are provided in Table S1. One-way ANOVAs were performed separately for each gene and each time point. If the ANOVA showed a $p \leq 0.05$ for effect of treatment, Dunnett's post-hoc test was performed to identify statistically different dose groups. Asterisks indicate groups that were statistically different from control ($p \leq 0.05$). (B) *atp2a2*; (C) *nac2*; (D) *ryr2*; (E) *myl7*; (F) *myh7*; (G) *nkx2.5*; (H) *notch1*; (I) *nrg2*; (J) *hbegfa*.

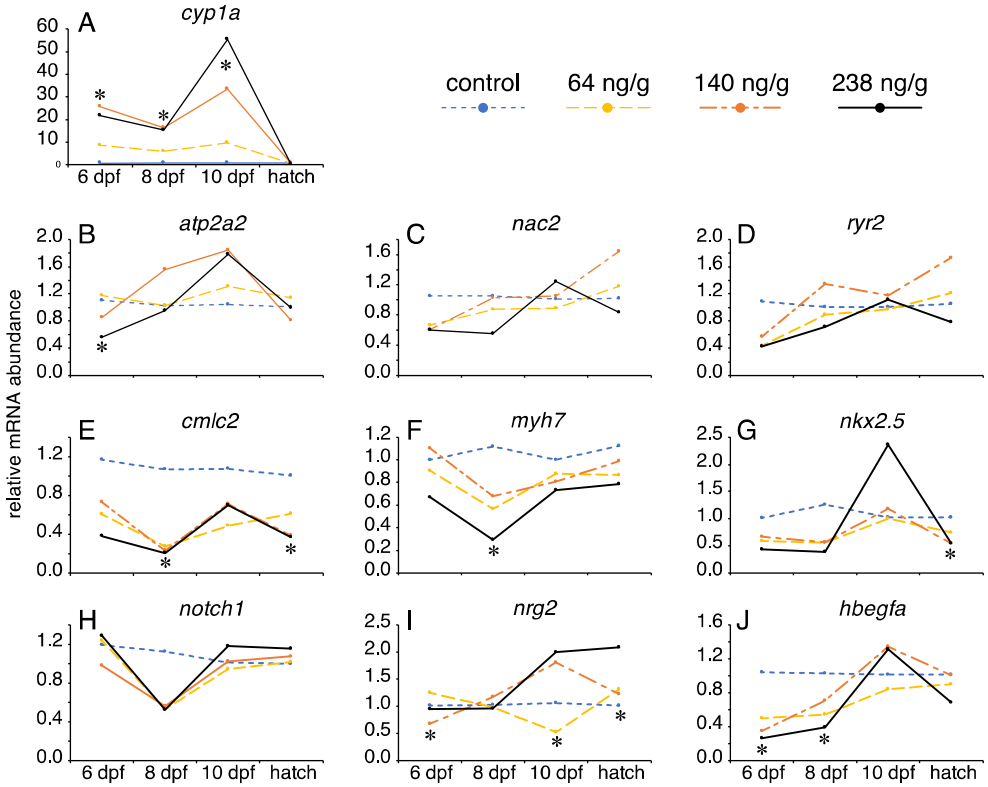
A
cyp1a
60
50
40
30
20
10
0
6 dpf
8 dpf
10 dpf
hatch
control
64 ng/g
140 ng/g
238 ng/g
relative mRNA abundance
B
atp2a2
C
nac2
D
ryr2
E
cmlc2
F
myh7
G
nkx2.5
H
notch1
I
nrg2
J
hbegfa

Figure 8: Model summarizing the adverse outcome pathway for low-level crude oil toxicity during fish embryonic development. *MIE*, molecular initiating event; *KE*, key event; *AO*, adverse outcome. Gene expression markers identified in this study are indicated in the boxes along the far right.